

Searching for active low-mass stars in CMa star-forming region: multi-band photometry with T80S

J. GREGORIO-HETEM,¹ F. NAVARETE,¹ A. HETEM,² T. SANTOS-SILVA,¹ P.A.B. GALLI,³ B. FERNANDES,¹ T. MONTMERLE,⁴
V. JATENCO-PEREIRA,¹ M. BORGES FERNANDES,⁵ H. D. PEROTTONI,¹ W. SCHOENELL,⁶ T. RIBEIRO,⁷ AND A. KANAAN⁸

¹Universidade de São Paulo, IAG, Rua do Matão 1226, 05508-090 São Paulo, Brazil

²UFABC Federal University of ABC, Av. dos Estados, 5001, 09210-580 Santo André, SP, Brazil

³Laboratoire d'Astrophysique de Bordeaux, Univ. Bordeaux, CNRS, B18N, Allée Geoffroy Saint-Hilaire, 33615 Pessac, France

⁴Institut d'Astrophysique de Paris, France

⁵Observatório Nacional, Rua General José Cristino 77, 20921-400, Rio de Janeiro, Brazil

⁶GMTO Corporation 465 N. Halstead Street, Suite 250 Pasadena, CA 91107

⁷Rubin Observatory Project Office, 950 N. Cherry Ave., Tucson, AZ 85719, USA (AURA Staff)

⁸Departamento de Física, Universidade Federal de Santa Catarina, Florianópolis, SC, 88040-900, Brazil

(Received MM dd, 2020; Revised MM dd, 2020; Accepted MM dd, 2020)

Submitted to AJ

ABSTRACT

An exotic environment surrounds the young stellar groups associated with the Canis Major (CMa) OB1/R1 region, which probably was formed under feedback from at least three supernova events having occurred a few million years ago. We use astrometric data from the *Gaia*-DR2 to confirm the membership of the stars in CMa R1, based on proper motion and parallax, which revealed 514 new members and candidates. The mean age of 5 Myr estimated from the color-magnitude diagram characterizes the sources as likely pre-main sequence candidates. In total, a sample of 694 stars detected with the *T80*-South telescope was analyzed according to different color-color diagrams, which were compared with theoretical colors from evolutionary models, aiming to reveal the objects that exhibit color excess due to accretion processes. Accretion and magnetic activity were also explored on the basis of empirical flux-flux relation, such as F_{660} and F_{861} that are related to $H\alpha$ and Ca II triplet emission, respectively. A low fraction (~ 3 percent) of the sample have $H\alpha$ excess and other colors expected for stars exhibiting chromospheric activity. The number of Class I and Class II objects, identified by the infrared (*WISE*) colors, indicates a disk fraction of ~ 6 percent, which is lower than the expected for stellar clusters with similar age. A such large sample of objects associated with CMa R1 without evidences of circumstellar accretion can be interpreted as a lack of disk-bearing stars, unusual for young star-forming regions. However, this may be explained as the result of supernova events.

Keywords: stars: pre-main sequence – ISM: clouds – open clusters and associations: general.

1. INTRODUCTION

Depicting different scenarios of star formation can bring us important clues for answering some of the major problems in astrophysics, mainly related with the early evolution of stars and protoplanetary disks, with implications on planet formation as well as on the structure and evolution of the Galaxy.

Despite the impressive progress that star formation study has achieved thanks to the advances on multi-band observational data analysis, there are still many open questions related to the physical relation between young star clusters and their respective parental clouds.

Our long-term goal is to study the young stellar population in different Galactic regions, and investigate the influence of the environment and feedback from massive stars (ionization, winds, supernovae) in the formation and evolution of star clusters and circumstellar disks. This work is focused on the star-forming region Canis

Major (CMa) R1 region, aiming to improve the census of the young stellar population.

The CMa OB1/R1 Association is a large (~ 100 deg²) complex of molecular clouds, emission and reflection nebulae showing evidences of star formation induced by supernova explosions. In a search for emission-line stars, [Shevchenko et al. \(1999\)](#) found about two hundred B stars associated with the reflection nebulae that constitute the CMa R1 region, located at $d \sim 1$ kpc (for a review, see [Gregorio-Hetem 2008](#)).

CMa R1 has a mixing of young objects with ages ranging from 1 to 10 Myr, distributed on a large scale region ([Gregorio-Hetem et al. 2009](#)). Based on X-ray observations in the direction of the Sh 2-296 nebula, [Santos-Silva et al. \(2018\)](#) reported more than 300 low-mass young stars candidates. As noted by [Fernandes et al. \(2015\)](#), among the T Tauri stars found by them around Sh 2-296, less than 10 percent show evidence of circumstellar disks. Such low fraction of disk-bearing stars is quite rare when compared with other star-forming regions ([Haisch et al. 2001](#); [Hernández et al. 2008](#); [Fedele et al. 2010](#); [Cloutier et al. 2014](#); [Briceño et al. 2019](#)), suggesting that some external factor accelerated the disk dissipation. More recently, [Fernandes et al. \(2019\)](#) identified three runaway stars associated with bow-shock structures in CMa OB1/R1 region. Those authors found that the runaway stars have likely been ejected from three successive SN explosions (~ 6 , ~ 2 and ~ 1 Myr ago), which might have originated the arc-shaped structure named “CMa shell” by them.

In this work we explore the importance of large-scale, multi-wavelength surveys to characterize the pre-main sequence stars associated with CMa R1 in order to investigate aspects such as disk evolution. The goal is to analyze a large reliable sample of members, providing a new optical characterization complemented with the classification based on infrared-excess. By these means, the fractions of accreting stars and disk-bearing stars can be inferred and compared with other stellar clusters with similar age.

The paper is presented as follows. In Sect. 2 we describe the data that we obtained from previous works, and from observations developed by us with the *T80*-South telescope. We also use proper motion and parallax from the *Gaia*-DR2 catalog to select the sample containing the probable members associated with CMa R1. The criteria for sample selection and classification are presented in Sect. 3, while the methods based on diagnosis of accretion and magnetic activity, which were adopted to analyze the sample, are described in Sect. 4. Finally, in Sect. 5 we summarize and discuss the main results.

2. OBSERVATIONS

2.1. Data from previous works

To better understand the star formation scenario and the early evolutionary stages of the stars associated with CMa OB1/R1 we previously analyzed the X-ray sources detected by *ROSAT* and *XMM-Newton* satellites in the direction of the nebula Sh 2-296 ([Gregorio-Hetem et al. 2009](#); [Santos-Silva et al. 2018](#)). The characterization of the X-ray sources was based on *2MASS* data of their near-infrared counterparts for which mass and age were estimated. This analysis indicates they are probably pre-main sequence stars, but their nature needs to be confirmed by means of complementary optical data.

For a small part (12 percent) of the area where the X-ray sources are found, [Fernandes et al. \(2015\)](#) obtained medium-resolution optical spectra with GMOS (multi-object spectroscopy) at the Gemini telescopes. The GMOS data were used to obtain the spectral classification of the candidates as a diagnosis of their youth nature based on the H α and lithium lines. The near- to mid-infrared data extracted from *2MASS* and *All-WISE* catalogues were used to search for evidences of circumstellar structure, which had indicated a low fraction of disk-bearing stars as reported by [Fernandes et al. \(2015\)](#). A similar result was found by [Fischer et al. \(2016\)](#) who adopted the criteria from [Koenig & Leisawitz \(2014\)](#) for distinguishing Class I, II and III objects that respectively are embedded, disk-bearing, and disk-lacking stars. [Fischer et al. \(2016\)](#) found a few groups of Class I or Class II stars over the entire area of CMa OB1/R1. These groups are shown in Fig. 1, together with the distribution of dust (WISE image) and molecular clouds (CO map) of the region.

Figure 1 also shows the regions covered by different surveys performed by us to study the CMa R1 region: optical spectroscopy with Gemini telescopes ([Fernandes et al. 2015](#)), *XMM-Newton* ([Santos-Silva et al. 2018](#)), and optical photometry obtained with *T80*-South telescope (see Sect. 2.2). In spite of the fact that intermediate-mass stars are well known in this region ([Shevchenko et al. 1999](#); [Gregorio-Hetem et al. 2009](#)), the sample of fainter, low-mass stars is still incomplete.

According to the literature, in the area covered by the *T80*-South observations (red square in Fig. 1), there are 430 stars that are likely associated with the CMa R1 region. Among those previously known objects, 60 corresponds to B- or A-type stars ([Claría 1974](#); [Shevchenko et al. 1999](#)) and 370 are young low-mass stars candidates selected from *XMM* data ([Santos-Silva et al. 2018](#)). However, 64 percent of them does not fulfill the parallax

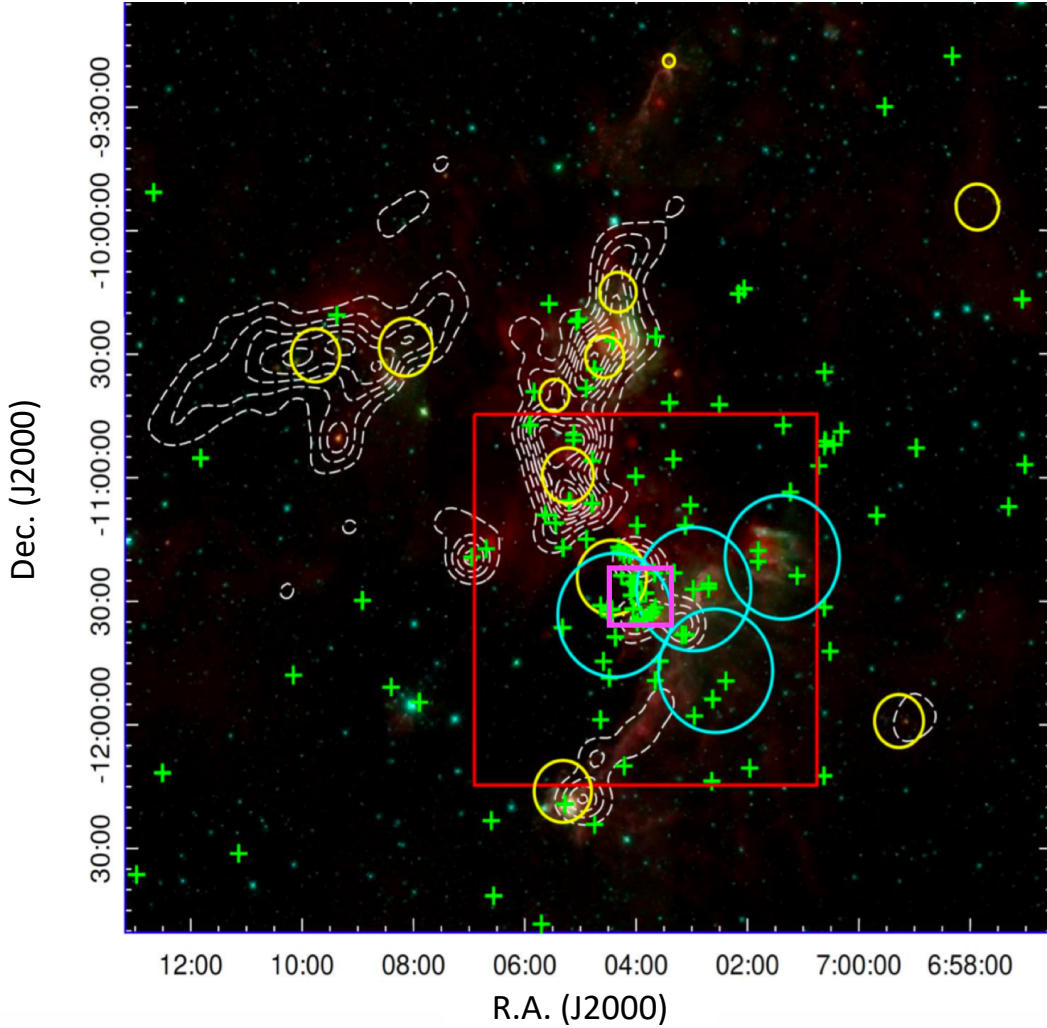


Figure 1. Infrared (*WISE*, $22\ \mu\text{m}$) image of CMa R1 region overlapped with ^{13}CO map (dashed contours) from Osaka group (see Onishi et al. 2013), showing the position of B-type stars (green crosses, Shevchenko et al. 1999), and groups of Class I and Class II stars (yellow small circles, Fischer et al. 2016). The fields covered by our observational campaigns are also indicated: *T80S* (red large box), *XMM-Newton* (cyan circles), and GMOS (pink small box).

and kinematic criteria used to confirm their association with CMa R1 (see further discussion in Sect. 3.1).

Therefore, the optical observations from *T80*-South combined with *Gaia* data analyzed in this work aim both purposes: (i) complementing the characterization of the candidates found by *XMM* around Sh 2-296, which is necessary to confirm if they are Pre-Main Sequence (PMS) stars, and (ii) seeking the detection of young star candidates in a larger area of the CMa R1 region. Figure 1 (right panel) provides a comparison of the areas covered by our observations showing the distribution of candidates that are X-ray sources ($\sim 0^\circ.5 \times 1^\circ.3$), and the confirmed PMS stars, which were observed by GMOS ($\sim 0^\circ.23 \times 0^\circ.33$). This illustrates the gain of *T80*-South observations to identify PMS member candidates across this OB association in a much larger area than the pre-

vious follow-up spectroscopic study of Fernandes et al. (2015).

2.2. Multi-band photometry with *T80S*

Optical imaging in a wide ($1^\circ.4 \times 1^\circ.4$) field-of-view (FoV), covering the CMa R1 region was performed in 2017, 17 January, with the 0.8-meter telescope *T80*-South (hereafter *T80S*) located at Cerro Tololo (Chile). *T80S* is dedicated to performing the “Southern Photometric Local Universe Survey” (S-PLUS) (for more details see Mendes de Oliveira et al. 2019). S-PLUS uses five broadband SDSS filters (u' , g' , r' , i' , z') and seven narrow-band filters centered on features particularly interesting for our study, like Ca II H+K ($\lambda = 3968.5\text{\AA}$, 3933.7\AA), H α ($\lambda = 6562.8\text{\AA}$), and Ca II infrared triplet (IRT, $\lambda = 8498\text{\AA}$, 8542\AA , 8662\AA), among others. A set of three images was obtained for each of the 12 filters.

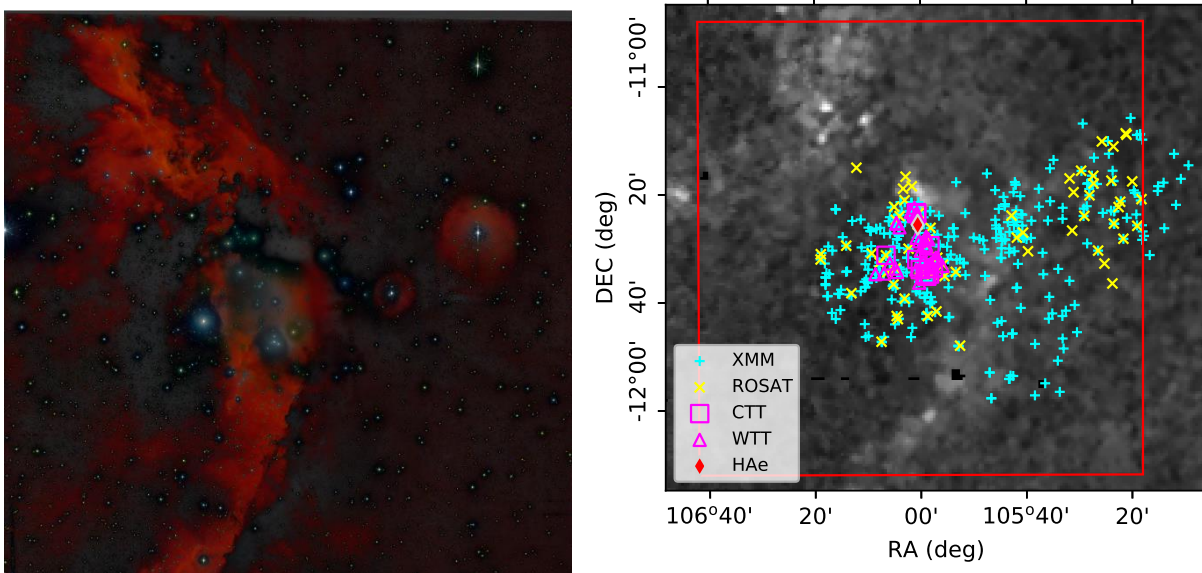


Figure 2. *Left panel:* Combined image of filters J0660 ($H\alpha$, red), r' (green), and g' (blue) obtained with *T80S* observations. The field has $1^\circ.4$ each side. North is up and East is to the left. *Right panel:* Visual extinction (A_V) map of CMa R1 overlapped by the *T80S* FoV (red square), and the position of X-ray sources from Santos-Silva et al. (2018, *XMM-Newton*) and Gregorio-Hetem et al. (2009, *ROSAT*). Pink symbols show the previously known PMS stars (Fernandes et al. 2015, *GMOS*). Inverse scale of colors is used for the map, where dense regions appear in white and light grey indicates low level of extinction ($A_V < 1$ mag).

Table 2 presents details of data acquisition in the CMa R1 region.

Figure 1 (left panel) shows a false-color composite RGB image combining three filters, enhancing the nebular ($H\alpha$) emission associated with Sh 2-296. For comparison with the dust distribution in the cloud, the right panel of Fig. 1 displays the visual extinction map (Gregorio-Hetem 2008) towards the area covered by *T80S*. The position of the X-ray candidates is also shown to indicate the area covered by *ROSAT* and *XMM* observations (Gregorio-Hetem et al. 2009; Santos-Silva et al. 2018). Different symbols are used to show where the previously known PMS stars are located.

The data¹ extraction and calibrations procedures were performed by the S-PLUS team, which developed a pipeline based on the *SExtractor* software (Bertin & Arnouts 1996; Bertin 2010) to construct the photometric catalogues (Mendes de Oliveira et al. 2019). The S-PLUS pipeline provides a first estimate of the flux corresponding to the zero-point of magnitude, to be used in the conversion of instrumental magnitudes.

By adopting the mean values of zero-point (ZP_o) magnitudes estimated by the S-PLUS team² as a first guess, we obtained a preliminary catalogue of about 73700

sources extracted from the *T80S* images. In Sect. 4.1 we present details on the photometric calibration and selection of the sub-sample that is analyzed in this work. The astrometry of the detected sources was checked by comparing their position with the known emission-line stars from Shevchenko et al. (1999).

3. SAMPLE SELECTION AND CLASSIFICATION

The main selection criterion is based on the second GAIA data release (*Gaia*-DR2, Gaia Collaboration et al. 2018a), which was used to confirm the membership of the objects associated with the nebula, and to exclude sources detected by the *T80S* that are likely field-stars in the line-of-sight of the CMa R1 region (Sect. 3.1).

Infrared and optical colors were used in order to classify the new PMS members and candidates, as well as the previously known candidates, in comparison with confirmed PMS objects. Firstly we search for sources exhibiting infrared (IR) excess based on data from the *WISE* survey (Sect. 3.2), and secondly we estimate ages using the *Gaia*-DR2 (Sect. 3.3).

3.1. Selection of kinematic members

The query was restricted to the sources in the parallax range $\varpi = 0.8 - 1.25$ milliarcseconds (mas) that is consistent with the distance of the cloud ($d \sim 1$ kpc, Gregorio-Hetem 2008). To avoid objects showing low quality of the astrometric solution, we applied the se-

¹ Data reduction is made using the J-PLUS pipeline (Cenarro et al. 2019)

² ZP_o calculated by L. San Pedro (private communication).

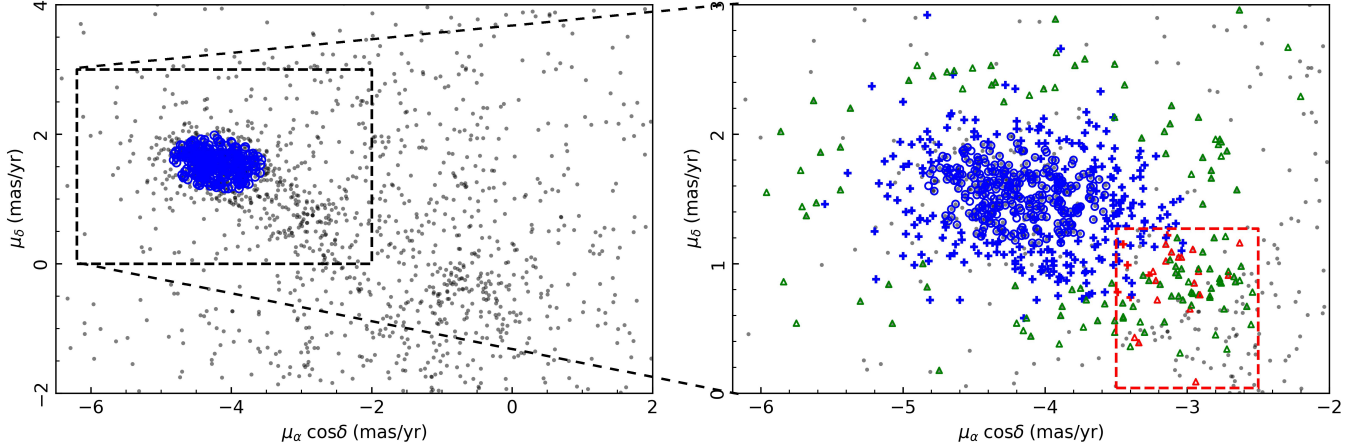


Figure 3. *Left:* Sources selected from *Gaia*-DR2 (gray dots) for which we estimate membership probabilities based on proper motion. Blue circles indicate very-likely members with $P \geq 90$ percent. *Right:* a zoom of the main clustering of objects observed by both *GAIA* and *T80S* surveys. The membership $50 \leq P < 90$ percent defines the probable members (blue +), while and candidates (green triangles) have $P < 50$ percent. The sources in the apparent sub-cluster (dashed red box) may be part of a group (highlighted by red symbols) that is located to the NW direction of the region (see Fig. 5.)

lection criteria of $\varpi/\sigma_\varpi > 3$ and $\text{RUWE}^3 < 1.4$ that resulted in an initial list of 4153 objects found in the *T80S* FoV.

For estimation of membership probability (P) we adopted the method from [Hetem & Gregorio-Hetem \(2019\)](#) combining a Bayesian model and the Cross Entropy (CE) technique to identify cluster members based on their proper motion ($\mu_\alpha \cos \delta$, μ_δ). Due to the high sensitivity of this method to initial conditions, we used a Genetic Algorithm presented by [Hetem & Gregorio-Hetem \(2007\)](#) to estimate optimized initial values required to create the first generation of parameters for the CE.

The result of the CE method gives the range of proper motion $\mu_\alpha \cos \delta = -4.1 \pm 0.6 \text{ mas yr}^{-1}$, $\mu_\delta = 1.5 \pm 0.4 \text{ mas yr}^{-1}$ that was adopted as criterion to select the stars probably associated with the CMa R1 region. According to the proper motion criterion, 78 percent of the objects extracted from *Gaia*-DR2 probably are field stars ($P < 1$ percent). The remaining list to be studied contains about 900 *Gaia* sources, 281 of them are very-likely members ($P \geq 90$ percent), which can be seen in the $\mu_\alpha \cos \delta$ - μ_δ plot presented in Fig. 3 (left panel).

To produce the final list of objects, we performed a cross-matching of the sources selected from *Gaia* with our preliminary catalog of objects detected with *T80S*. For the 281 *Gaia* sources with membership $P \geq 90$ percent, we have found 208 cross-matching pairs in the *T80S* catalog, meaning that 73 very likely members were

missed in the source extraction performed by the *T80S* team that uses an automatic pipeline, which is based on aperture photometry. We adopted the Star Finder (SF) procedure ([Diolaiti et al. 2000](#)) on three *T80S* images (filters J0430, J0515, and J0660), seeking for sources that are absent in our preliminary catalog.

The cross-matching of our preliminary catalogue and the list obtained with SF is illustrated in Fig. 4. The magnitudes found by adopting both techniques are in agreement for sources brighter than 20 mag at 660 nm, showing a dispersion of 0.5 mag (or more) in the case of fainter magnitudes. This result gives us confidence in considering in our analysis the list of sources produced by SF, which were missed in the preliminary catalogue. These additional sources were included in our list that contains 669 selected objects: 281 members ($P \geq 90$ percent), 242 probable members ($50 \leq P < 90$ percent), and 146 candidates ($P < 50$ percent).

Figure 3 (right panel) illustrates our selection criterion that is based on the above mentioned range of proper motion. In the plot centre there is a main clustering where the very-likely members are concentrated (inside an ellipse of 1σ size). Around the main clustering we selected the probable members and candidates, which are contained in a 3σ distribution that overlaps an apparent sub-cluster (seen to the right). Objects in this sub-cluster may be part of a group located to the NW direction that was identified by Santos-Silva et al. (2020, hereafter SS20) based on a clustering code that uses 5-dimensional data from *Gaia*-DR2 to diagnose physical groups in the direction of the CMa OB1 stellar association.

³ Re-normalised unit weight error (see details in the technical note GAIA-C3-TN-LU-LL-124-01)

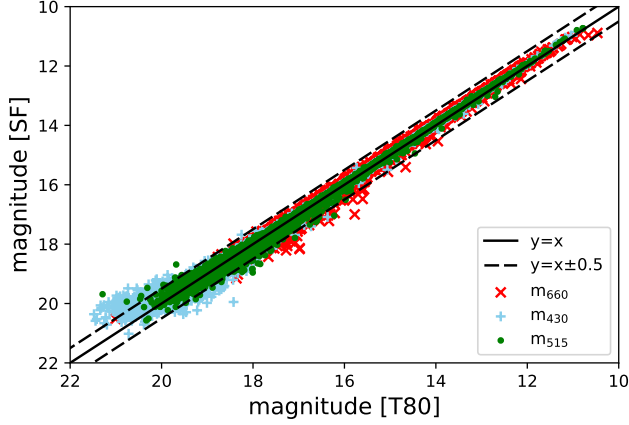


Figure 4. Comparison of magnitudes obtained with filters J0660, J0515 and J0430, by using two different extraction methods: automatic procedure performed by the *T80S* team and StarFinder (SF) routine adopted by us. A dispersion is found for the faintest sources ($m_{430} > 20$ mag.)

Table 1 summarizes the astrometric and kinematic parameters of our sample, compared with the results for two groups found by SS20. The proper motion and parallax of those groups coincide with the range adopted here to select members and candidates: our main clustering has parameters similar to those estimated by SS20 for the group called CMa06, while the sub-cluster seen in Fig. 3 may be part of other group called CMa05.

A view of the distribution of the sample in the equatorial coordinates space is presented in Fig. 5. As expected, it can be noted a clear main concentration of sources at the center, tending to the E direction of the observed region, and roughly following the arc-shaped nebula shown in Fig. 1. According to Gregorio-Hetem et al. (2009), there is a mixing of objects with ages from 1 to 10 Myr in this area that includes the sources at the NW direction. In Sect. 3.3 we revisit these population differences, exploring our sample of young candidate members that is larger than those previously studied.

The list of objects that were previously identified in the literature and were extracted from the *Gaia*-DR2 according to our selection criteria contains 155 objects. Table 3 gives the kinematic data for 149 of these known objects that were also identified in our *T80S* catalog. The last lines of Table 3 present the six objects not found in the *T80S* catalog, probably due to saturation (for bright objects), low S/N photometry in the case of faint sources, or nebular contamination.

For comparison purposes, we also analyzed 37 confirmed PMS stars, which were classified by Fernandes et al. (2015) according to $H\alpha$ and Li lines detected in *GMOS* spectra. However, only 6 of them are listed

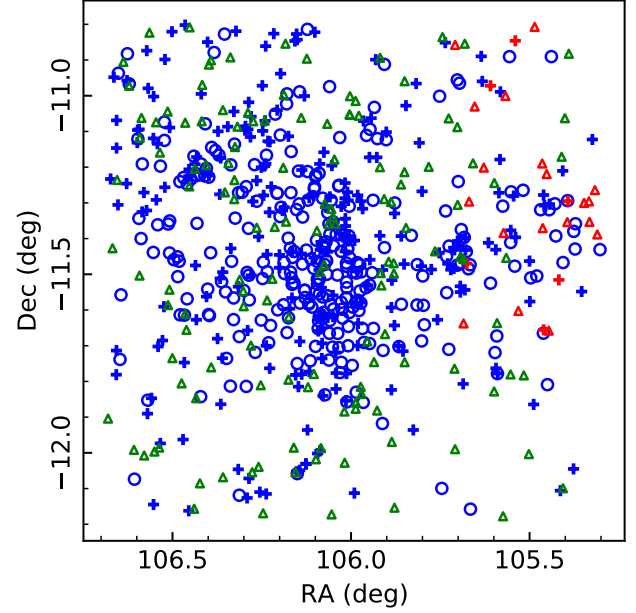


Figure 5. Distribution of candidates and members in the area covered by *T80S* observations. The symbols are the same used in Fig. 3. In the NW region we use red symbols to highlight the sources appearing in the sub-cluster seen in Fig. 3.

Table 1. Parameters related to the *Gaia*-DR2 data analysis

ID	RA	Dec	ϖ	$\mu_{\alpha} \cos \delta$	μ_{δ}
	J2000	J2000	mas	mas yr^{-1}	mas yr^{-1}
<i>T80S</i> _{total} ^a	106°0±0.7	-11°5±0.7	0.8 - 1.25	-4.1±0.6	1.5±0.4
<i>T80S</i> _{sub} ^{a,b}	105°5±0.2 -0.2	-11°3±0.5 -0.3	0.9±0.1	-3.1±0.2	0.9±0.3
CMa06 ^c	106°2±0.2	-11°4±0.3	0.85±0.09	-4.2±0.4	1.5±0.2
CMa05 ^c	105°3±0.2	-11°2±0.2	0.76±0.09	-3.0±0.1	0.8±0.1

NOTE— (a) This work; (b) sub-structure seen in Fig. 3; (c) Results from other work (SS20) that identified two clusters coinciding with our sample.

in Table 3, while the other sources do not fulfill our selection criteria, and/or have poor photometry (mentioned above). To take in account the other 31 known PMS stars that were missing, it was necessary to relax the kinematic criteria in the *Gaia* data query, and also to adopt a lower threshold limit to extract their *T80S* fluxes. Table 4 gives the list of these objects: 7 Classical T Tauri stars (CTT), 23 weak-line T Tauri stars (WTT), and one Herbig Ae star (HAe).

In total, our final sample contains 694 objects, which are analyzed in this work. Besides the 180 stars previously identified (149+31, above mentioned), there are 514 objects that we suggest to be new young stars associated with CMa R1. Among the new stars identified

in this work, 395 are probable members ($P \geq 50$ percent) for which we present the *Gaia*-DR2 data in Table 5, while 119 are candidates ($P < 50$ percent) presented in Table 6.

3.2. Infrared excess

Part of our sample was previously studied in order to search for disk-bearing stars among the candidates revealed by *XMM-Newton* data from Santos-Silva et al. (2018), focusing on 205 X-ray sources exhibiting a single IR counterpart (Gregorio-Hetem et al. 2016). The IR colors were compared to the criteria suggested by Koenig & Leisawitz (2014) to distinguish different PMS classes using *WISE* photometric bands (Wright et al. 2010), according with the distribution of stars studied in Taurus by Rebull (2010). Only a small fraction (16/205) of our X-ray sources were considered disk-bearing candidates, according to their position in the Class II expected locus. Most (92%) of the IR counterparts of the *XMM* sources in CMA have *WISE* colors of diskless (Class III) objects.

Here, we extend the same analysis for a larger and more reliable sample in which membership is confirmed by kinematic criteria. Figure 6 shows the $[3.4] - [4.6] \times [4.6] - [11.6]$ diagram of 79 known objects from Table 3, and 357 new members and candidates (Tables 5 and 6) identified with good IR photometric data in the *All-WISE* Catalog, according with the mitigation and contamination filters proposed by Koenig & Leisawitz (2014, see their Sect. 2.3). We also plot 26 previously confirmed PMS stars, but in this case, no photometric quality filter was used. Only two objects coincide with the Class I region: a new member, and the Herbig Ae star identified by Fernandes et al. 2015). The Class II locus in Fig. 6 is occupied by six T Tauri stars; 11 known candidates; and 24 new members (Tables 5 and 6). In summary, a total of 43 objects were identified in Fig. 6, from which 41 correspond to Class II and two are Class I objects. These sources exhibiting IR excess are highlighted in the following figures.

Taking into account the number of objects with available *WISE* photometry (463 objects), the fraction of disk-bearing stars (Class I or II) is $43/463 \sim 9$ percent. This is an upper limit, since there are other 206 objects of our entire sample that do not have *WISE* data. It is tempting to suggest these remaining stars probably are Class III, assuming that a lack of data could be due to fainter IR emission. If this hypothesis is correct, the fraction of disk-bearing stars drops to $43/694 \sim 6$ percent.

3.3. Ages

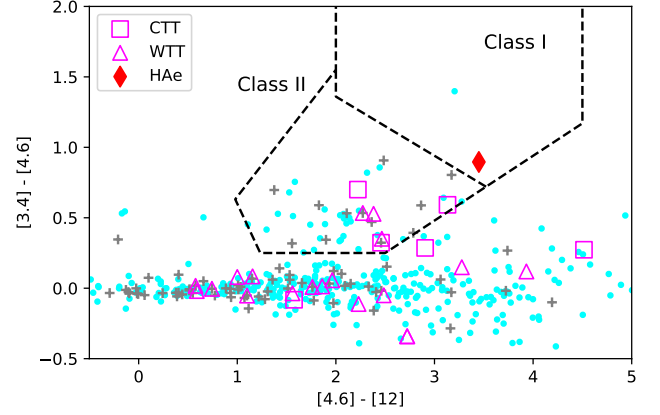


Figure 6. *WISE* color-color diagram obtained for our sample: new members (cyan dots); previously known candidates (grey +); and the T Tauri stars (pink) and one H Ae star (red diamond) spectroscopically confirmed by Fernandes et al. (2015). Dashed lines indicate the expected locus of Classes I and II young stars (Koenig & Leisawitz 2014). The objects outside these boundaries probably are Class III (disk-lacking) stars.

The second step for classifying our sample was to determine the range of the stellar ages using *Gaia*-DR2 photometry. Figure 7 presents the magnitude-color diagram constructed using the G_{Gaia} magnitude as a function of the $[G_{BP}] - [G_{RP}]$ color. In the same plot, we compare the distribution of the points with isochrones from *PARSEC*⁴ (Bressan et al. 2012; Marigo et al. 2017). The models for 1 Myr and 5 Myr were adopted to respectively indicate the young- and intermediate-ages, expected for the CMA R1 population (see discussion below). The 100 Myr isochrone was chosen to represent the ZAMS (Zero Age Main Sequence) aiming the comparison with the Main Sequence (MS) colors used by other works discussed in Sect. 4.2.

Most of the T Tauri stars; other previously known objects, and sources exhibiting IR excess (Class II) are ~ 5 Myr or younger. About half of the new members and candidates presented in here are in the same range of ages, while the other half are older, but still in the PMS phase.

It is interesting to discuss the spread of ages in comparison with the kinematic characteristics presented in Sect. 3.1. As previously noted by Gregorio-Hetem et al. (2009), CMA R1 has a mixed population. The sources found outside the nebula (to the W direction) tend to be in the 5-10 Myr range (or older), which can be explained by their location in a region depleted of gas, where the

⁴ Version v1.2S+COLIBRI PR16 of *PARSEC* models available on <http://stev.oapd.inaf.it/cgi-bin/cmd>.

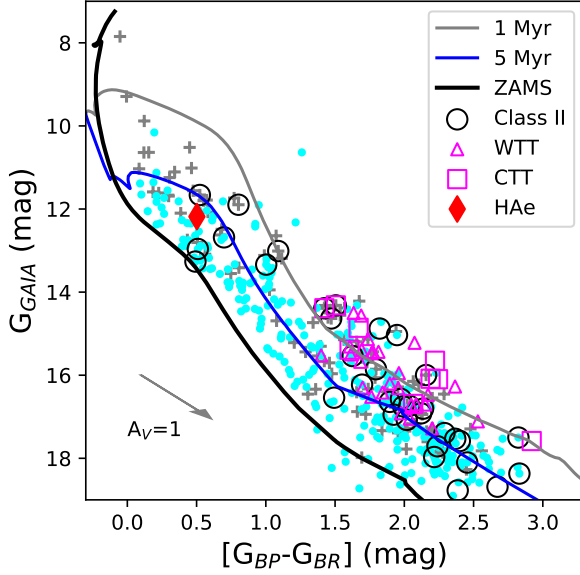


Figure 7. Color-magnitude diagram obtained from *Gaia*-DR2 photometry compared with isochrones from PARSEC. The symbols are the same as Fig. 6, with open circles to highlight the sources exhibiting IR-excess (Class II).

star formation seems to be ceased. This older group coincides with the sub-cluster CMa05 located to the NW direction (see Table 1) for which SS20 estimated an age of 25^{+3}_{-7} Myr.

On the other hand, the main clustering associated with the cloud tend to be younger. For the group CM06, which coincides with our main clustering of members, SS20 estimate a mean age of 6^{+1}_{-1} Myr. The method adopted by those authors is based on the *fitCMD* code from Bonatto (2019) that provides accurate age estimates for stellar clusters.

In summary, the age estimation obtained here is validated by other method, giving weight to the characterization of our sample as likely PMS members of CMa R1.

4. ANALYSIS

In this section we describe the methodology we adopted to explore the observational data of our targets, by highlighting some of the results from the literature that have inspired this work.

By comparing the photometric data at different bands, we are able to estimate colors of the sources in several spectral domains, which characterize the cloud members. In particular, the flux of H α and Ca II IRT features combined with u' , g' , r' colors, give us inferences on accretion rate and magnetic activity.

To identify sources showing color excess, it is necessary to refine the ZP magnitudes (mentioned in Sect.

Table 2. Details of the *T80S* observations.

filter	t_{exp}	seeing	m_{sat}	$m_{50\%}$	λ	ZP _o	ZP _f
	s	"	mag	mag	Å	mag	mag
u'	681	2.042	9.40	22.10	3574	19.64 ± 0.09	18.80
J0378	660	1.747	9.60	21.83	3771	19.07 ± 0.09	18.55
J0395	354	1.763	9.87	21.47	3941	19.09 ± 0.11	19.00
J0410	177	1.844	10.02	21.53	4094	20.10 ± 0.11	20.20
J0430	171	1.632	10.08	21.54	4292	20.26 ± 0.10	20.45
g'	99	1.772	10.06	21.88	4756	22.54 ± 0.09	22.74
J0515	183	1.639	9.95	21.33	5133	20.41 ± 0.08	20.65
r'	120	1.617	10.00	21.12	6260	22.46 ± 0.06	22.75
J0660	870	1.775	9.96	21.02	6614	19.95 ± 0.08	20.15
i'	138	1.620	10.01	20.54	7692	22.30 ± 0.06	22.44
J0861	240	1.397	10.02	20.23	8611	20.58 ± 0.07	20.70
z'	168	1.548	10.50	20.27	8783	21.75 ± 0.06	21.85

NOTE— Seeing indicates the quality of photometric observations. The saturation limit is given by m_{sat} and photometric depth is $m_{50\%}$. Last columns give the first estimate of Zero Point (ZP_o) and the adopted value (ZP_f), for which we assume uncertainty of 0.1 mag.

2.2) by comparing theoretical data with the observed (u' , g' , r' , i' and H α) color-color diagrams, as presented in the following subsection

4.1. Calibration

The data calibration and evaluation of ZP magnitudes were based on spectral energy distribution (SED) fitting and color-color diagram from g' -, r' -, and i' -band. We analyzed only sources exhibiting well-determined fluxes (signal-to-noise ratio S/N > 10) measured with the filter J0660. We also used the photometric depth of the S-PLUS images presented by Mendes de Oliveira et al. (2019), by selecting only sources that are brighter than 21.12 mag for r' -band, for instance, leading to a list of about 12,000 sources that have good photometric quality. Table 2 gives the $m_{50\%}$ photometric depth corresponding to the magnitudes at which 50 percent of the total detected sources are included. On the other hand, the upper limit of saturation is 10 mag at r' -band, which corresponds to the brighter source detected in the *T80S* image without indication of saturated pixels. In the observed field, there are only four B-type stars brighter than this limit that could be affected by saturation: HD 53396, HD 53456, HD 53457, for which no photometry was extracted from the *T80S* catalog, and HD 53035 that was detected with $r' = 9.03$ mag. Excepting these stars, the sources in our sample are fainter than the saturation limit (m_{sat}) given in Table 2.

Among the intermediate-mass stars from Shevchenko et al. (1999, SEI99) that were detected by *T80S*, we selected two to fit their SED: [S99]28 (spectral type B3) and [SEI99]160 (HT CMa; A0e), which were used as

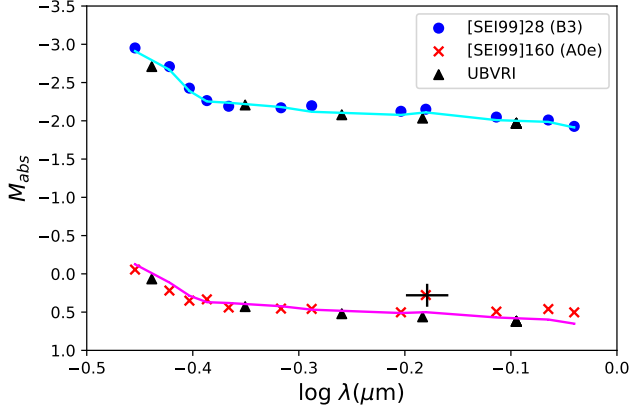


Figure 8. Absolute magnitudes (*S-PLUS* photometric system) provided by *PARSEC* models (ZAMS) for masses: $5 M_{\odot}$ (cyan line), and $3 M_{\odot}$ (pink line), compared with the *T80S* photometry obtained for two intermediate-mass stars from Shevchenko et al. (1999, SEI99). The SED fitting is also confirmed by adopting the theoretical colors from the *UBVRI* system (black triangles). As it is typical for Ae stars, [SEI99]160 shows excess at $H\alpha$ band, which is indicated by black error-bars.

calibration stars. The SED fitting was obtained by comparison of the observed absolute magnitudes with the theoretical values extracted from *PARSEC* model for the 100 Myr isochrone that was chosen to represent the ZAMS. Vega magnitudes from two photometric systems were adopted: *S-PLUS* and *UBVRI* (Maíz Appellániz 2006; Bessell 1990).

We found for [SEI99]28 a good match with the $5 M_{\odot}$ stellar model, while the magnitudes of [SEI99]160 are better represented by the $3 M_{\odot}$ model, excepting for an excess in $H\alpha$ noted for this star.

Figure 8 shows the theoretical SEDs compared with data of calibration stars. A best fitting was obtained by adopting $A_V = 0.3$ mag ([SEI99]28) and 1.0 mag ([SEI99]160) for reddening correction of the observed magnitudes. These A_V values agree well with the visual extinction map available for the CMA region (Gregorio-Hetem 2008). Based on the results of the SED fitting, we obtained the final values for ZP_f , which are reported in Table 2.

An independent validation of the ZP_f values was obtained by following Mendes de Oliveira et al. (2019, see also Molino et al. 2014) that give the transformations between magnitudes from *Gaia-DR2* and *T80S*, expressed by:

$$G_{T80S} = +2.0528 m_{660} - 1.0594 i' \quad (1)$$

$$G_{T80S} = -0.0372 m_{515} + 1.0442 r' \quad (2)$$

$$G_{T80S} = -1.7642 m_{430} + 2.7824 g' \quad (3)$$

where i' , r' , g' , m_{660} , m_{515} , and m_{430} are the apparent magnitudes measured in the respective bands and calibrated with the ZP_f given in Table 2.

Figure 9a shows the empirical G-band magnitudes (G_{T80S}) obtained by a linear fit of magnitudes from a set of *T80S* filters and the *Gaia-DR2* G-band magnitudes (G_{Gaia}). A good correlation of G_{T80S} with G_{Gaia} is obtained for most of the sources, which are found in between the dashed lines representing 0.5 mag deviation. The faint sources ($G_{T80S} > 16$ mag) show a dispersion, possibly due to different reasons (e.g. variability; photometric errors; etc). Figure 9b displays the distribution of mean values of errors as a function of observed magnitudes for each *T80S* filter, showing that sources fainter than 16 mag have errors larger than 0.05 mag. Bright sources (~ 8 mag) tend to show larger errors at filters F660 and F861 than those measured in other bands, probably due to nebular contamination combined with saturation effects.

Despite the dispersion of faint sources, the result shown in Fig. 9 can be considered as a validation of the ZP calibration adopted by us. Additional criteria confirming this hypothesis are discussed as follows.

4.2. Accretion

Venuti et al. (2014) used u , g , and r photometry to estimate accretion rates for the pre-main sequence population of the young cluster NGC 2264. The candidates showing UV-excess were selected from the $[u-g] \times [g-r]$ and $[r] \times [u-r]$ diagrams, where the Classical T Tauri stars (CTTs) occupy a distinguished locus, separated from weak-line T Tauri (WTTs) and field stars.

The $[u-g]$ color is also useful to distinguish candidates showing evidences of UV-excess due to accretion process. For instance, Kalari et al. (2015) obtained $H\alpha$ and u -band accretion rates for CTTs in the Lagoon Nebula M8 by using *ugri* and $H\alpha$ photometry from the VST Photometric $H\alpha$ survey (VPHAS+, Drew et al. 2014).

Following Venuti et al. (2014) and Kalari et al. (2015), we present our results in the diagrams shown in Fig. 10, by comparing the observed colors with theoretical MS and ZAMS (*PARSEC* model, Bressan et al. 2012), whose fitting may validate the ZP calibration. The previously known candidates exhibiting good quality photometry (see Sect. 4.1) are indicated by grey symbols, while cyan dots are used to show the new members and candidates.

We also highlight in Fig. 10 the distribution of PMS stars characterized on the basis of *GMOS* spectra (Fernandes et al. 2015).

In Fig. 10a, we compare $[r' - H\alpha] \times [r' - i']$ with MS colors given by Drew et al. (2014). According to Kalari et al. (2015) accreting stars are expected to be

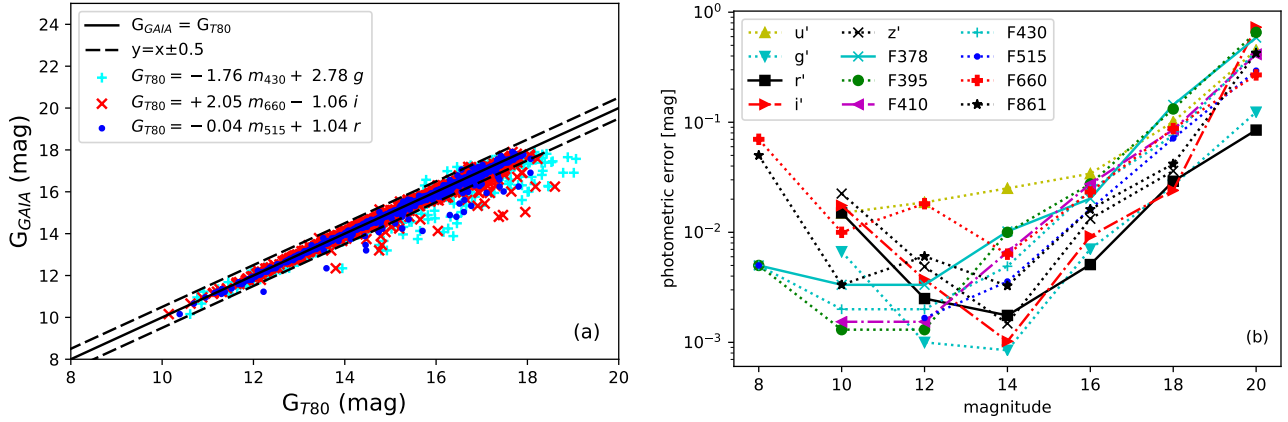


Figure 9. (a) Different relations used to transform *T80S* photometry into G-band magnitude of the *Gaia-DR2* system. (b) Distribution of mean photometric errors as a function of magnitude for each filter, presented in 2 mag wide bins: 7-9, 9-11, etc.

found above the MS line, in a locus where bluer sources ($[r' - i'] < 1$ mag) have $[r' - H\alpha] \gtrsim 0.5$ mag, and redder sources have $[r' - H\alpha] \gtrsim 0.8$ mag. The presence of objects at that region of the plot is interpreted as an evidence of $H\alpha$ excess related to accretion activity.

Here, we draw attention to 22 objects (marked with error bars) that appear with $H\alpha$ excess in Fig. 10a: six are known candidates and 16 are new members. Among them there are two Class II stars (black circles, see Sect. 3.2), and one Class I candidate (highlighted by a filled circle). However, no $H\alpha$ excess is clearly seen for the other sources having IR excess. Furthermore, none of the confirmed PMS stars can be used as indicator of accretion, since they are found below the MS. This is expected for the WTT stars, but it should not be the case for the HAe and the CTT stars. We tentatively suggest that it can be due to the low S/N photometry acquired for these faint sources (see Sect. 3.1).

Among the other candidates previously known that appear in the bottom of Fig. 10a there are two B-type stars listed by Shevchenko et al. (1999): [SEI99]102 and [SEI99]111, for the latter no $H\alpha$ emission was detected in previous studies (Cohen & Kuhi 1979; Wiramihardja et al. 1986; Shevchenko et al. 1999) or in the present work. The other stars located at this region of the plot are X-ray sources that could be WTTs, which typically do not exhibit strong $H\alpha$ emission.

Figure 10b is a color-magnitude diagram comparing the distribution of our sample and the MS line from Covey et al. (2007), by adopting the $[g'] \times [g' - i']$ magnitudes. The data points are also compared with the ZAMS that coincides with the MS in this plot, and the 5 Myr isochrone (*PARSEC*), representing a mean value of age estimated for the sample (see Fig. 7).

The observed $[g' - r'] \times [r' - i']$ colors compared with MS from Covey et al. (2007) are presented in Fig. 10c.

In a similar study, results from Venuti et al. (2014) show no-accreting stars (WTTs) coinciding with the MS, while CTTs are widely scattered around the MS. In our case, only a few objects are found below the MS curve, but we cannot be sure if this is related to accretion or not, since these stars may not exhibit u' -band excess.

Figure 10d presents the $[u' - g'] \times [g' - r']$ diagram used to verify the occurrence of UV-excess in our sample. We also compare our data with the ZAMS. Despite the large dispersion, probably due to low quality of photometry in the u' -band, most of the objects are likely following the theoretical ZAMS. Only a few stars are found below this curve, which is the expected locus of stars showing UV-excess (Kalari et al. 2015).

By considering only objects of our sample, we suggest that 3.2 ± 0.7 percent (22/694) seem to have accretion activity as indicated by both $[r' - H\alpha] \times [r' - i']$ and $[u' - g'] \times [g' - r']$ diagrams, which confirm our previous results about the lack of disk-bearing stars associated with Sh 2-296, which is the main nebula of CMA OB1/R1.

4.3. Magnetic Activity

Due to the lack of spectroscopic observations for our sample, we can not evaluate the spectral flux to probe magnetospheric accretion, nor to estimate accretion rates. Alternatively, we can obtain an indirect evidence of activity by using photometry taken at spectral bands containing the aimed spectral lines.

The measurements of $H\alpha$ flux, combined with the flux of Ca II lines is commonly used as indicators of chromospheric activity in late-type dwarf stars (see references given by Martínez-Arnáiz et al. 2011). The flux-flux relationship between $H\alpha$ and Ca II IRT (λ 8498 Å) evaluated by those authors shows that young stars have an excess of flux at these bands, when compared with the empirical linear fit found for F- G- and K-type active stars. Despite the differences on the considered wave-

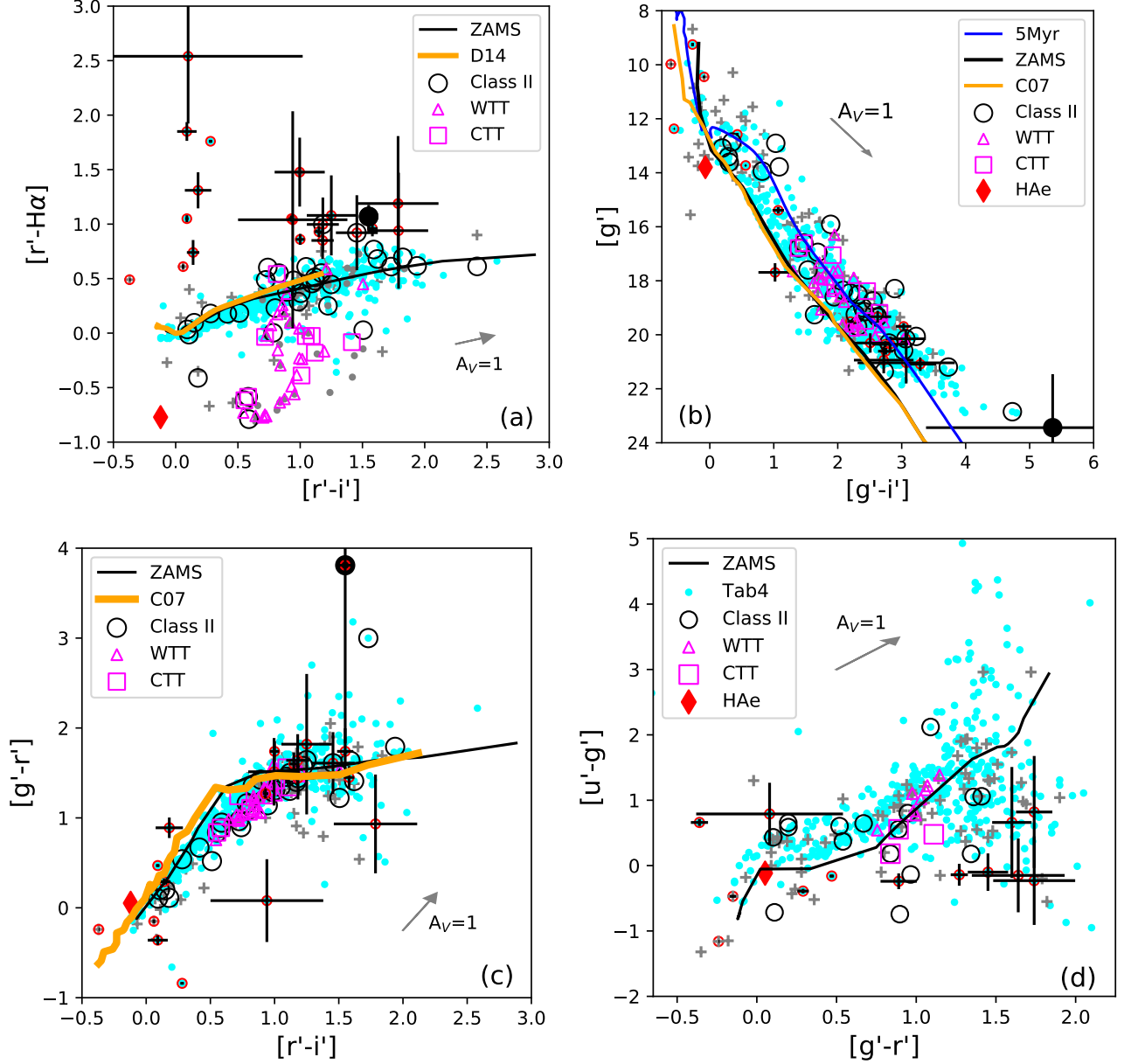


Figure 10. Color-color diagrams obtained for *T80S* data compared with theoretical colors from *PARSEC* model (ZAMS, black line), and the Main Sequence (orange line) from [Drew et al. \(2014, D14\)](#), or [Covey et al. \(2007, C07\)](#). The previously known candidates (grey +), and the confirmed PMS members ([Fernandes et al. 2015](#)) T Tauri stars (pink squares and triangles) and Herbig Ae star (red diamond) are listed in Table 7. The new members and candidates revealed in this work (cyan dots) are listed in Tables 8 and 9. Open black circles indicate the objects showing *WISE* colors typical of Class II stars (see Fig. 6), and a filled circle shows one Class I candidate. In panel (a) we note 22 objects exhibiting $[r' - H\alpha]$ color excess, which are marked by red circles with error-bars (for some of them the errors are lower than the symbol size).

length, we used magnitudes measured with filters J0660 and J0861 (see Table 2), aiming to roughly reproduce the flux-flux relationship between $H\alpha$ and Ca II IRT, respectively. It is important to note that we are not es-

timating line fluxes here, but just comparing broad band fluxes⁵, with no subtraction of continuum.

Figure 11 shows the flux-flux relationship between the fluxes F_{660} and F_{861} observed with *T80S*, showing a few

⁵ The conversion of instrumental magnitudes (m_λ) to flux (F_λ) is given by $F_\lambda(Jy) = 3631 \times 10^{-0.4[m_\lambda + (ZP_f)_\lambda]}$

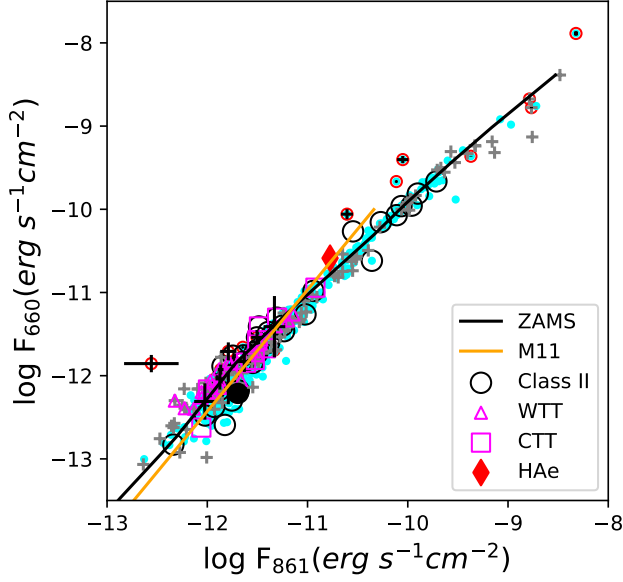


Figure 11. Broad band fluxes associated with the $H\alpha$ and Ca triplet emission, respectively estimated from the m_{660} and m_{861} magnitudes observed with *T80S*. The flux-flux relation is comparable with results from [Martínez-Arnáiz et al. \(2011, M11\)](#), where active late-type stars are expected to appear above the MS line. Symbols are the same as Fig. 10.

sources above the MS line that could indicate $H\alpha$ excess. This is not unexpected since most of the objects studied by [Fernandes et al. \(2015\)](#) are WTTs, and the A- and B-emission stars ([Shevchenko et al. 1999](#)) present in our sample are not strong $H\alpha$ emitters.

5. CONCLUSIONS

5.1. Summary of results

We used the *Gaia*-DR2 astrometric data to evaluate the membership probability (P) and identify the CMa R1 members based on proper motion. From *Gaia*-DR2 we extracted only the objects showing parallax $\varpi = 0.8 - 1.25$ mas, compatible with the distance of the cloud ($d \sim 1$ kpc, [Gregorio-Hetem 2008](#)), $RUWE < 1.4$ and $\varpi/\sigma_\varpi > 3$ resulting in a list of $\sim 4,200$ objects in the area observed with *T80S*.

Our *T80S* observations covered a ~ 2 deg² area around Sh 2-296, the main nebula of the CMa R1 region, where more than 70 thousand objects were detected, 17 percent of them exhibiting good quality photometry.

We selected 669 sources on the basis of membership probability that was estimated with the Bayesian technique. The mean values of proper motion for 523 probable members ($P \geq 50$ percent) are: ($\mu_\alpha \cos \delta \sim -4.1 \pm 0.6$, $\mu_\delta \sim 1.5 \pm 0.4$) mas yr⁻¹. We also considered 146 candidates ($P < 50$ percent) exhibiting proper motion compatible within a 3σ -interval from the mean values. The

other objects extracted from *Gaia* are very likely field-stars (membership probability: $P < 1$ percent).

Table 3 contains 155 stars that are candidates previously identified in the literature, but only 149 were included in our final sample because six sources were not detected by *T80S*. Other 31 previously known objects included in our sample are spectroscopically confirmed PMS stars (Table 4), but they have low S/N photometry. In total, our final sample contains 694 sources, 180 of them are previously known objects. Therefore, the membership analysis based on *Gaia*-DR2 data revealed 395 new members (not previously identified in the literature) and 119 new candidates. Table 5 and Table 6 give the kinematic data and identification of these new members and candidates, respectively.

The color-magnitude diagram $G_{Gaia} \times [G_{BP} - G_{RP}]$ was used to estimate the age of the sources. A mean value of 5 Myr was found, which characterizes our sample as likely PMS members of CMaR1. The presence of IR-excess was investigated on the basis of *WISE* colors that revealed 43 objects: 2 are Class I and 42 are Class II. Only six of the T Tauri stars have IR-colors typical of Class II (none is Class I), which indicates that most of the confirmed PMS stars of our sample are Class III, exhibiting low IR emission.

The photometric zero-points (ZPs) and calibration of the *T80S* data were obtained by using different methods (see Sect. 4.1). First, we performed the SED fitting of two stars with well determined spectral type, by adopting *PARSEC* evolutionary models.

The ZPs were also evaluated by analyzing the g', r', i' colors diagram and correlations between the G-band magnitude from *Gaia*-DR2 (G_{Gaia}) and empirical values obtained from *T80S* data (G_{T80}).

Table 7 gives the photometric data for previously known objects that were observed by *T80S*. The photometric data for the new members and candidates are given in Tables 8 and 9, respectively.

Color-color diagrams were used to confirm the occurrence of CMa R1 members showing color excess related to accretion process, which did not reveal more than 22 stars with excess in the $H\alpha$ or the u' -band.

Magnetic activity was investigated according the flux-flux relations used by [Martínez-Arnáiz et al. \(2011\)](#) comparing $H\alpha$ and Ca II H & K lines fluxes typically found for late-type stars showing chromospheric activity. An excellent correlation between the broad band F_{660} and F_{861} fluxes is found, but only a few stars have indications of $H\alpha$ excess likely due to accretion.

5.2. Concluding remarks

Previously we identified a few hundred young stars candidates associated with the nebulae in CMa R1, but our studies were restricted to small areas, such as the fields covered by *XMM-Newton* observations. Aiming to explore a more complete and reliable sample of candidates, the *Gaia*-DR2 catalog was used to select the kinematic members, for which we analyzed multi-band *T80S* imaging observations that provided very good indicators of accretion activity.

Despite a large sample of new PMS candidates were identified, a small fraction of them show signs of accretion processes and/or magnetic activity. Only 3.2 ± 0.7 percent of our sample seem to have H α and/or UV excess, which gives an estimation of accreting fraction.

Based on the number of Classes I and II sources (43/694) we estimate a disk fraction of 6.2 ± 0.9 percent. We have noticed in our sample the presence of sources that may be part of a sub-group, which was identified in the NW direction of the region. But none of these sources have IR-excess. Therefore, the number of disk-bearing stars is evaluated here for the whole population.

Comparing CMa R1 with other regions, we note that our results are lower than the values expected for young stellar groups with similar ages (~ 5 Myr). For instance,

a disk fraction of more than 10 percent is reported for NGC 2362 (Haisch et al. 2001); and 20 percent for Upper Sco (Fedele et al. 2010; Cloutier et al. 2014). The accretion fraction estimated for these regions is ~ 5 percent (Fedele et al. 2010). More recently, Briceño et al. (2019) presented the decline of the accreting fraction, as well as the percentage of disk-bearing stars, as a function of the mean age of each sub-group of the Orion OB1 star-forming region. For Orion_{1b} sub-group that is 5 Myr old, they report an accreting fraction of about 10 percent, and a disk fraction of ~ 15 percent.

We conclude that analyzing the optical photometric data gave us a confirmation of our previous results, which were based on spectroscopy and near-infrared data. Despite the use of a much large sample of candidates, the absence of disk-bearing stars in the region is confirmed. Somehow, circumstellar accretion has finished for the young stars in this region, probably due to the star formation scenario where at least three supernova events occurred a few millions years ago. This could be the cause of the disks disappearance earlier than usually is found in other star-forming regions at same age.

Table 3. Objects identified in the literature, giving membership probability (P%), parallax (ϖ), proper motion ($\mu_\alpha \cos \delta$ and μ_δ), and other data from *Gaia*-DR2.

<i>Gaia</i> -DR2	2MASS	RA degree	Dec degree	P %	ϖ mas	$\mu_\alpha \cos \delta$ mas yr ⁻¹	μ_δ mas yr ⁻¹	G mag	Note
3046091622096649600	07013441-1117375	105.3934	-11.2938	96	0.912±0.042	-4.110±0.072	1.459±0.067	15.3	W011a
3046093301427017600	07013774-1112371	105.4072	-11.2104	81	0.89±0.21	-3.72±0.41	2.01±0.39	15.77	W096
3046095195509364608	07013843-1110147	105.4102	-11.1708	0	1.104±0.107	2.395±0.199	-6.209±0.190	17.33	W076
3046063893787827840	07014236-1123337	105.4265	-11.3927	94	0.986±0.088	-4.354±0.143	1.762±0.167	16.94	W021
3046088937740213888	07014669-1118126	105.4445	-11.3035	86	0.87±0.15	-3.48±0.27	1.39±0.26	17.74	W038
3046088976396774016	07015002-1118275	105.4584	-11.3077	54	0.805±0.028	-3.569±0.048	2.023±0.048	13.95	W047a
3046089148195449472	07015058-1116405	105.4608	-11.278	89	0.975±0.048	-4.044±0.087	1.928±0.083	15.54	W005
3046088770238881024	07015256-1119089	105.469	-11.3192	95	0.912±0.026	-4.060±0.046	1.694±0.048	13.41	W016
3046010425734094208	00000000-0000000	105.5315	-11.6026	2	0.947±0.268	-2.939±0.419	0.088±0.397	18.6	S119
3046040593585163008	07021265-1122366	105.5527	-11.3769	85	0.862±0.136	-4.030±0.242	2.054±0.273	17.57	C078
3046040288648050688	07021274-1124394	105.5531	-11.411	95	0.830±0.047	-3.883±0.075	1.467±0.082	15.7	W046
3045994658915621120	07021278-1146494	105.5533	-11.7804	0	1.126±0.051	-1.544±0.076	-2.312±0.073	12.62	S006
3045995517909047040	07022324-1143091	105.5968	-11.7192	92	0.848±0.116	-4.164±0.176	1.215±0.185	16.41	S019
3045991356082680576	07022386-1149410	105.5994	-11.8281	0	1.12±0.05	-2.29±0.08	2.67±0.07	11.01	[SEI99]52 (B8-9)
3046035164747476224	07024001-1128240	105.6667	-11.4733	94	0.916±0.101	-3.908±0.177	1.440±0.193	17.17	C041
3046035272126240640	07024222-1128112	105.6759	-11.4698	59	0.88±0.19	-3.40±0.39	0.74±0.42	18.51	C042b
3046037608588438400	07024252-1126118	105.6772	-11.4366	95	0.879±0.036	-3.883±0.067	1.407±0.070	11.74	[SEI99]160(Ae)
3046038016604720000	07024312-1123532	105.6797	-11.3981	66	0.860±0.124	-3.178±0.222	1.436±0.282	17.6	C026b
3046037608588436224	07024314-1125544	105.6797	-11.4318	88	0.851±0.087	-3.646±0.174	1.746±0.212	16.92	C035
3046038020905285376	07024393-1123475	105.6831	-11.3965	95	0.890±0.049	-3.921±0.084	1.518±0.109	17.6	C026a
3046035306485972608	07024398-1127282	105.6832	-11.4579	73	0.892±0.041	-4.020±0.073	0.977±0.076	11.01	C001a
3046035302188600448	07024458-1127264	105.6858	-11.4573	26	1.11±0.34	-3.24±0.68	-0.21±0.81	18.24	C001c
3046035302185109888	07024607-1128059	105.692	-11.4683	92	0.849±0.053	-3.887±0.104	1.222±0.110	16.06	C015
304602593382800384	07024652-1132594	105.6939	-11.5498	80	0.858±0.084	-3.941±0.159	0.986±0.167	16.55	C033
3046036779655724544	07024651-1127040	105.6939	-11.4512	0	1.08±0.25	9.27±0.46	-14.62±0.51	18.66	C023C ^c
3046037746027380992	07024757-1125096	105.6982	-11.4194	87	0.941±0.090	-3.502±0.156	1.385±0.191	16.95	C020a
3046047779070945024	07024832-1118203	105.7014	-11.3056	1	1.136±0.038	-4.153±0.063	0.483±0.081	15.22	C021b
3046037780387115520	07024842-1124244	105.7017	-11.4068	77	0.809±0.119	-3.713±0.228	0.941±0.278	17.29	C017
3045992734767643648	07025047-1145520	105.7103	-11.7644	0	0.91±0.10	-5.18±0.13	10.93±0.16	16.54	S002b ^c
3046037711667638144	07025410-1125160	105.7254	-11.4211	91	0.881±0.160	-3.927±0.269	1.797±0.321	18.25	C044
3046036676574755968	07030077-1126239	105.7532	-11.44	83	1.224±0.223	-3.576±0.364	1.184±0.446	18.62	C006
3046050837087595008	07030776-1111569	105.7824	-11.1992	0	1.038±0.046	6.711±0.080	-6.378±0.084	7.85	[C74]72; [SEI99]72; HD53035(B1)
3046017950516574592	07031077-1138285	105.7949	-11.6413	95	0.949±0.042	-4.023±0.072	1.364±0.079	10.52	[SEI99]73 (B3)
3046021631310115840	07031139-1135127	105.7974	-11.5869	95	0.907±0.034	-3.864±0.057	1.387±0.064	14.56	C025
3046024483168373248	07031181-1130169	105.7992	-11.5047	90	0.907±0.110	-3.889±0.178	1.161±0.221	16.71	C031
3046024586247581312	07031269-1128382	105.8029	-11.4773	88	0.903±0.061	-3.768±0.106	1.174±0.124	16	C029

Table 3 continued

Table 3 (continued)

<i>Gaia-DR2</i>	2MASS	RA degree	Dec degree	P %	ϖ mas	$\mu_{\alpha} \cos \delta$ mas yr ⁻¹	μ_{δ} mas yr ⁻¹	G mag	Note
3046024964204699392	07031553-1128219	105.8147	-11.4728	95	0.920±0.077	-4.112±0.130	1.696±0.152	16.77	C097
3046043067485306368	07031952-1123282	105.8313	-11.3912	94	0.846±0.039	-4.426±0.062	1.343±0.079	11.56	[SEI99]77 (B3)
3046020016402397184	07032616-1135024	105.859	-11.584	90	0.819±0.150	-4.210±0.295	1.179±0.331	17.86	C067
3046031419534969472	07032626-1123349	105.8594	-11.3931	88	0.982±0.163	-3.983±0.268	1.108±0.277	17.82	C059
3046045614407372032	07033309-1117510	105.8879	-11.2975	8	0.900±0.054	-4.959±0.087	2.415±0.094	16.15	C032
3046030113863947136	07033469-1127533	105.8946	-11.4648	0	1.180±0.040	-2.201±0.070	2.291±0.068	12.49	C071
3045829178114006656	07033845-1142477	105.9102	-11.7132	92	0.897±0.113	-3.770±0.193	1.391±0.234	17.39	E076a
3046020703597135488	07033961-1131526	105.9151	-11.5313	0	1.046±0.052	-0.055±0.075	0.021±0.073	11.61	[SEI99]82 (B8)
3046026884049098112	07034002-1129480	105.9168	-11.4966	0	1.062±0.058	-2.632±0.105	2.958±0.099	16.34	C057
3046031526914666496	07034064-1123314	105.9193	-11.3921	89	1.002±0.040	-4.803±0.069	1.784±0.078	11.8	[SEI99]84; C043 (A)
3046026853990282496	07034583-1129446	105.941	-11.4957	95	0.89±0.06	-3.88±0.10	1.62±0.10	16.13	E077
3046027060148696320	07034733-1127333	105.9472	-11.4592	89	0.84±0.07	-4.71±0.12	1.32±0.12	16.46	E173
3046020669237386624	07034751-1131489	105.9479	-11.5302	96	0.94±0.06	-4.34±0.13	1.61±0.12	15.95	C051a
3046019913323141504	07034869-1131502	105.9529	-11.5306	85	0.91±0.08	-4.83±0.14	1.33±0.14	16.71	E039
3045830964820569344	07035234-1139061	105.9681	-11.6517	93	0.876±0.064	-4.615±0.131	1.674±0.151	16.23	E142
3046026750911057408	07035303-1129352	105.971	-11.4931	94	0.851±0.032	-4.584±0.050	1.689±0.056	14.39	E065a; F13 (CTT)
3046019535363545472	07035324-1134449	105.9718	-11.5792	62	1.12±0.18	-4.65±0.29	2.46±0.36	17.87	E107a
3046019531067048320	07035338-1134504	105.9724	-11.5807	94	0.83±0.04	-4.59±0.07	1.62±0.08	15.38	E107b
3046025720119222784	07035400-1132478	105.975	-11.5466	95	0.821±0.031	-4.562±0.053	1.535±0.052	14.32	E056; F14 (CTT)
3046027163227907840	07035414-1128235	105.9756	-11.4732	90	0.94±0.10	-4.68±0.34	1.33±0.21	16.33	E015b
3045831759397198080	07035472-1136057	105.978	-11.6016	92	0.87±0.09	-4.66±0.15	1.42±0.15	17.06	E074
3046027163227906432	07035503-1128181	105.9793	-11.4717	93	0.83±0.07	-4.69±0.18	1.65±0.15	16.52	E015a
3045831072202462848	07035523-1138157	105.9801	-11.6377	83	0.813±0.100	-4.997±0.182	1.749±0.172	16.82	E079
3045829796589332992	07035555-1141594	105.9815	-11.6998	76	0.897±0.268	-3.909±0.540	0.752±0.688	18.78	E031C
3046026716551315072	07035575-1129315	105.9823	-11.4921	85	0.837±0.041	-4.587±0.068	1.185±0.070	15.13	E017; F20a (WTT)
3046027163227903872	07035584-1128029	105.9827	-11.4675	93	0.88±0.11	-4.17±0.24	1.26±0.20	16.94	C047b
3046026716547544704	07035646-1129476	105.9852	-11.4966	94	1.20±0.11	-4.59±0.19	1.62±0.18	17.06	E378a
3045831862476390144	07035666-1134553	105.9861	-11.5821	85	0.87±0.07	-4.34±0.12	1.09±0.12	16.08	E099
3046032042310727040	07035770-1124199	105.9904	-11.4055	83	0.812±0.052	-4.844±0.079	1.907±0.080	12.64	E042
3046025960637068160	07035859-1129377	105.9941	-11.4938	96	0.852±0.032	-4.361±0.055	1.440±0.058	14.63	E078
3045831793756916736	07035880-1135311	105.995	-11.592	95	1.042±0.053	-4.424±0.089	1.469±0.087	11.24	[SEI99]95; E016a; F27 (WTT)
3046429721921201664	07040073-1100041	106.0031	-11.0012	0	0.907±0.061	-0.983±0.077	-1.419±0.072	11.11	[SEI99]101 (B6-8)
3046027300666846336	07040086-1127142	106.0036	-11.4539	90	0.862±0.033	-4.196±0.068	1.927±0.065	14.69	E085
3046027536887737984	07040225-1125429	106.0094	-11.4286	95	0.856±0.042	-4.465±0.089	1.429±0.099	12.18	E036b
3046027541185004416	07040234-1125393	106.0097	-11.4276	94	0.836±0.042	-4.534±0.075	1.388±0.070	10.64	[SEI99]99; E036a; F40 (B3-5)
3046025582680267904	07040284-1132155	106.0118	-11.5376	94	0.827±0.042	-4.439±0.070	1.337±0.070	11.67	[SEI99]100; E057a (B8-9)
3045837772351358976	07040285-1133579	106.0118	-11.5661	95	1.00±0.11	-4.32±0.18	1.44±0.18	17.05	E019b
3046027128868157696	07040309-1128071	106.0129	-11.4686	96	0.90±0.04	-4.25±0.07	1.60±0.06	15.31	E075
3045837772351358336	07040330-1133586	106.0138	-11.5663	95	0.86±0.07	-4.33±0.11	1.45±0.12	16.2	E019a

Table 3 continued

Table 3 (continued)

<i>Gaia-DR2</i>	2MASS	RA degree	Dec degree	P %	ϖ mas	$\mu_{\alpha} \cos \delta$ mas yr ⁻¹	μ_{δ} mas yr ⁻¹	G mag	Note
3046032076670456064	07040390-1123480	106.0162	-11.3967	88	0.92±0.06	-4.79±0.10	1.37±0.10	16.31	E043b
3046027330725137024	07040393-1126097	106.0164	-11.436	88	0.849±0.044	-4.338±0.082	1.151±0.076	9.88	[SE199]102;E002a
3045826502357320064	07040649-1144473	106.027	-11.7465	90	0.923±0.047	-4.044±0.081	1.160±0.086	15.96	E127
3046028812495321344	07040669-1126084	106.0279	-11.4357	96	0.834±0.039	-4.428±0.067	1.577±0.067	11.66	[SE199]162(B5e)
3046032660785990656	07040707-1121393	106.0295	-11.3609	94	1.16±0.14	-3.89±0.21	1.62±0.19	17.36	E140a
3046029254874690304	07040742-1123127	106.0309	-11.3869	85	1.04±0.27	-4.81±0.43	1.96±0.37	17.68	E014a
3045824165895135872	07040744-1146306	106.031	-11.7752	92	1.127±0.156	-3.905±0.273	1.479±0.328	17.94	E096
3045830277630801664	07040892-1139560	106.0372	-11.6656	94	0.89±0.09	-4.37±0.16	1.39±0.17	17.3	E113b
3046026098076337536	07040918-1130075	106.0383	-11.5021	91	0.82±0.05	-4.74±0.09	1.74±0.08	15.89	E020a
3046028945633705088	07041176-1125125	106.049	-11.4201	93	0.95±0.09	-4.60±0.17	1.69±0.16	17.25	E081
3046032626426246144	07041191-1121312	106.0496	-11.3587	88	0.880±0.032	-4.863±0.057	1.736±0.055	14.22	E038
3045732081796540544	07041306-1210207	106.0544	-12.1724	10	0.881±0.045	-3.453±0.079	0.696±0.091	11.03	[SE199]108(B6-8)
3046033034445913472	07041323-1119009	106.0551	-11.3169	1	0.888±0.040	-5.629±0.067	2.259±0.062	11.78	[SE199]111(B8)
3045837463113703424	07041357-1135085	106.0566	-11.5857	90	0.918±0.080	-4.809±0.136	1.695±0.137	16.88	E108
3046029568409539328	07041424-1123169	106.0594	-11.388	95	0.86±0.11	-4.29±0.18	1.69±0.14	16.74	E154
3045827361350689152	07041458-1139547	106.0608	-11.6652	95	0.87±0.10	-4.42±0.17	1.54±0.17	17.09	E129
3046029671488742144	07041484-1121315	106.0619	-11.3588	90	0.870±0.069	-4.545±0.118	1.897±0.110	16.57	E205b
3046029774567956736	07041523-1121326	106.0635	-11.3591	0	0.864±0.153	-2.849±0.253	-1.147±0.227	17.98	E205a
3046028121003292544	07041591-1126137	106.0663	-11.4371	79	0.90±0.13	-5.07±0.24	1.83±0.22	15.44	E111b
3045837669272106496	07041595-1133363	106.0665	-11.5601	94	0.883±0.109	-4.146±0.206	1.713±0.190	17.18	E087a
3046026128134299264	07041626-1129598	106.0677	-11.5	96	0.850±0.038	-4.299±0.067	1.598±0.066	12.07	E177
3046027919142464640	07041638-1127455	106.0683	-11.4627	96	0.921±0.052	-4.325±0.092	1.646±0.090	16.06	E120a
3046027914841395328	07041673-1127371	106.0697	-11.4603	90	1.009±0.234	-3.957±0.442	1.670±0.436	18.68	E120b
3046408380224749312	07041763-1118091	106.0734	-11.3025	17	0.878±0.041	-4.376±0.073	2.380±0.067	11.9	[SE199]116(A1)
3046027712984035584	07041779-1128212	106.0741	-11.4725	95	0.863±0.107	-4.184±0.219	1.517±0.210	17.28	E141a
3046027708686433152	07041804-1128239	106.0752	-11.4733	7	0.830±0.200	-4.745±0.432	0.176±0.400	18.27	E141b
3046028159660628352	07041812-1125280	106.0755	-11.4244	94	0.86±0.04	-4.47±0.07	1.80±0.06	15.39	E030a
3046028159660627968	07041839-1125239	106.0766	-11.4233	94	1.05±0.10	-4.48±0.17	1.75±0.15	16.91	E030b
3045836393659287936	07041898-1137255	106.0791	-11.6238	94	1.029±0.134	-4.110±0.241	1.440±0.240	17.78	E105
3045837978509746176	07041912-1133480	106.0797	-11.5634	96	0.864±0.041	-4.220±0.074	1.572±0.072	15.44	E012; F50 (WTT)
3046408487602990848	07041913-1117130	106.0797	-11.287	93	0.890±0.043	-4.687±0.066	1.702±0.064	12.1	[SE199]117(A0)
3046028159660626688	07041923-1125077	106.0801	-11.4188	96	0.833±0.037	-4.323±0.060	1.697±0.058	14.73	E004
3045825849522247296	07041959-1144087	106.0816	-11.7358	59	0.871±0.114	-3.098±0.189	1.475±0.201	17.34	E128
3045838077286610176	07041999-1132150	106.0833	-11.5375	86	0.81±0.15	-3.97±0.28	2.01±0.27	17.47	E122
3046029289231133056	07042018-1124325	106.0841	-11.4091	80	1.01±0.13	-4.49±0.21	2.11±0.19	17.2	E071
3045836432321555584	07042063-1136443	106.086	-11.6123	92	0.936±0.092	-4.185±0.158	1.885±0.162	17.35	E033
3045839971374505856	07042086-1129361	106.0869	-11.4934	24	0.825±0.058	-3.269±0.109	0.870±0.101	16.33	E143
3045836428019042304	07042103-1136565	106.0876	-11.6157	81	0.81±0.21	-4.98±0.35	1.40±0.39	18.47	E007b
3045836432321559040	07042135-1137043	106.089	-11.6179	93	0.828±0.026	-4.475±0.044	1.821±0.045	14.32	E007a

Table 3 continued

Table 3 (continued)

<i>Gaia-DR2</i>	2MASS	RA degree	Dec degree	P %	ϖ mas	$\mu_{\alpha} \cos \delta$ mas yr ⁻¹	μ_{δ} mas yr ⁻¹	G mag	Note
3045827430070138112	07042202-1139318	106.0918	-11.6588	83	0.89±0.10	-4.94±0.17	1.41±0.17	17.33	E126
3045827498789608832	07042210-1139067	106.0921	-11.6519	94	0.909±0.036	-4.472±0.057	1.373±0.063	10.64	[SE199]119(B5)
3045838184668136320	07042250-1131400	106.0938	-11.5278	96	0.805±0.041	-4.345±0.072	1.575±0.071	15.51	E013
3045838425187624960	07042264-1130482	106.0944	-11.5134	96	0.836±0.045	-4.324±0.081	1.624±0.094	15.62	E049
3046028571977483904	07042325-1124172	106.0969	-11.4048	95	0.844±0.054	-4.255±0.091	1.760±0.081	15.86	E047
3045838008567383424	07042340-1132515	106.0975	-11.5477	94	0.984±0.044	-4.348±0.068	1.312±0.068	15.47	E024; F55 (CTT)
3045836943420055424	07042820-1134486	106.1175	-11.5802	94	0.982±0.102	-4.423±0.172	1.425±0.176	17.57	E018b
3045837291314948736	07043096-1133542	106.129	-11.5651	96	0.836±0.038	-3.969±0.063	1.500±0.059	11.69	[SE199]123(B5-7)
3045837394386880768	07043099-1132417	106.1292	-11.545	96	0.853±0.057	-4.408±0.097	1.640±0.090	16.4	E035b
3045837390096654592	07043129-1132402	106.1304	-11.5445	90	0.81±0.24	-4.62±0.40	1.64±0.39	16.4	E035a
3046028228380101376	07043345-1126304	106.1394	-11.4418	88	0.806±0.099	-4.474±0.161	1.984±0.137	16.45	E098a
3045836909055443840	07043428-1134501	106.1429	-11.5806	95	0.850±0.085	-4.061±0.145	1.445±0.138	17.28	E064; F72 (CTT)
3045840658569185536	07043946-1126126	106.1644	-11.4369	83	1.00±0.12	-4.21±0.20	1.02±0.19	17.33	E203
3045837050796757760	07043968-1133593	106.1654	-11.5665	85	0.90±0.09	-4.50±0.16	1.13±0.15	17.36	E112
3045839009301795840	07044011-1130333	106.1672	-11.5093	95	0.869±0.028	-4.562±0.045	1.508±0.043	13.19	E132
3045833992780064768	07044125-1135469	106.1719	-11.5964	89	1.102±0.168	-4.748±0.267	1.796±0.263	18.15	E100
3045833683542438144	07044185-1137104	106.1744	-11.6196	41	1.12±0.13	-3.93±0.21	2.36±0.21	18.05	E041a
3045833610520490240	07044200-1137191	106.175	-11.622	94	0.863±0.040	-3.936±0.063	1.740±0.064	15.66	E041b
3045839352899157248	07044469-1129527	106.1862	-11.498	95	0.842±0.044	-4.494±0.069	1.720±0.063	15.44	E135
3046433845089734912	07044736-1056174	106.1973	-10.9382	73	0.872±0.026	-3.305±0.037	1.256±0.037	13.12	[SE199]131
3046418280128313088	07044755-1106364	106.1981	-11.1101	95	0.853±0.034	-3.897±0.047	1.489±0.045	13.09	[SE199]129
3046407388089313024	07045365-1115189	106.2235	-11.2553	84	0.918±0.053	-3.725±0.074	1.888±0.075	11.59	[SE199]132(B6-7)
3045832687110012800	07045407-1138362	106.2253	-11.6434	96	0.893±0.035	-4.321±0.059	1.468±0.072	15.15	E070
3045839284181079552	07045632-1129332	106.2347	-11.4926	96	0.895±0.031	-4.022±0.046	1.602±0.046	13.01	E021
304583367169540352	07045640-1134229	106.235	-11.573	0	0.953±0.068	-4.051±0.103	-2.572±0.114	16.46	E029a
3046214629962281472	07045894-1127572	106.2456	-11.4659	95	0.996±0.081	-3.909±0.129	1.564±0.116	16.75	E124
3045834198938470528	07050033-1137419	106.2514	-11.6283	96	0.868±0.033	-4.065±0.063	1.510±0.062	15.19	E045
3045819630409471360	07050441-1143071	106.2684	-11.7187	96	0.873±0.030	-4.170±0.054	1.502±0.047	14.38	E001
3045820420683429120	07050727-1141589	106.2803	-11.6997	0	0.950±0.022	-2.699±0.040	3.232±0.037	13.55	E151
3046211571945562752	07050985-1129411	106.291	-11.4947	96	0.846±0.036	-4.175±0.057	1.686±0.056	14.95	E054
3045834675672073728	07051217-1135218	106.3006	-11.5894	2	0.850±0.036	-2.771±0.058	0.885±0.059	12.74	E202a
3045835156708838400	07051248-1132500	106.302	-11.5472	0	0.806±0.066	-3.927±0.094	2.888±0.091	16.28	E121
3046211292766550400	07051489-1130542	106.312	-11.5151	0	0.895±0.040	-5.075±0.062	0.539±0.062	12.81	E134
3046210506793689856	07051571-1132050	106.3155	-11.5347	81	0.864±0.030	-4.721±0.051	1.200±0.048	14.61	E073
3046218787490488960	07051851-1117221	106.3271	-11.2895	0	1.247±0.073	-1.525±0.093	3.288±0.082	9.29	[C74]98; [SE199]144; HD53622 (B5V)
3046091617799837056	07013419-1117417	105.3925	-11.2950	61	0.89±0.22	-3.27±0.39	0.91±0.35	18.45	W011b
3046029117435703040	07040267-1124244	106.0111	-11.4068	89	0.95±0.25	-4.67±0.45	1.72±0.41	18.75	E068b
3046028159660628224	07042071-1125537	106.0862	-11.4317	60	0.98±0.32	-3.03±0.62	1.16±0.68	15.56	E147
3045813308217786880	07042891-1148578	106.1205	-11.8161	31	1.11±0.05	-4.11±0.09	2.30±0.09	9.69	[SE199] 112; HD 53396 (B9)

Table 3 continued

Table 3 (*continued*)

<i>Gaia-DR2</i>	2MASS	RA	Dec	P	ϖ	$\mu_{\alpha} \cos \delta$	μ_{δ}	G	Note
		degree	degree	%	mas	mas yr ⁻¹	mas yr ⁻¹	mag	
3045838837503121280	07043829-1131265	106.1596	-11.5241	91	0.89±0.05	-4.66±0.09	1.36±0.08	7.33	[C74] 92; [SEI99] 164; HD 53456; E009 (B0V)
3045805852154672128	07043847-1159075	106.1603	-11.9855	0	0.81±0.04	-0.61±0.08	-0.43±0.08	9.27	[C74] 90; [SEI99] 125; HD 53457 (B6-7)

NOTE— Objects from Fernandes et al. (2015) are indicated by letter F. X-ray sources are denoted by letters E, W, C, and S corresponding to fields East, West, Center and South (see Fig. 1) observed by *XMM-Newton* (Santos-Silva et al. 2018). Other identifications and Spectral Type were compiled by Gregorio-Hetem (2008) mainly from Claria (1974, C74) and Shevchenko et al. (1999, SEI99). The six objects in the bottom lines were not found in the *T80S* catalog.

Table 4. The same as Table 3, with the list of confirmed PMS stars (Fernandes et al. 2015).

<i>Gaia-DR2</i>	2MASS	RA degree	Dec degree	ϖ mas	$\mu_{\alpha} \cos \delta$ mas yr ⁻¹	μ_{δ} mas yr ⁻¹	G mag	Notes
3046019531067048320	07035338-1134504	105.9724	-11.5807	0.83 ± 0.04	-4.59 ± 0.07	1.62 ± 0.08	15.38	F10b (CTT)
3045831862476398336	07035542-1135149	105.9809	-11.5875	0.84 ± 0.09	-3.83 ± 0.15	0.47 ± 0.15	16.10	F18 (CTT?)
3045831862476390144	07035666-1134553	105.9861	-11.5820	0.87 ± 0.07	-4.34 ± 0.12	1.09 ± 0.12	16.08	F23 (CTT)
3045837772351364864	07040041-1133596	106.0017	-11.5666	0.68 ± 0.13	-4.74 ± 0.22	1.12 ± 0.25	15.65	F30 (CTT)
3046032179749669888	07040314-1123275	106.0131	-11.3910	0.50 ± 0.27	-5.43 ± 0.51	3.86 ± 0.47	17.58	F36c (CTT)
304602582680267776	07040290-1132074	106.0121	-11.5354	1.38 ± 0.27	-5.11 ± 0.49	1.51 ± 0.47	16.69	F37 (CTT)
3045838219027859456	07042625-1131207	106.1094	-11.5224	14.86	F60 (CTT?)
3046027536887737984	07040225-1125429	106.0094	-11.4286	0.86 ± 0.04	-4.46 ± 0.09	1.43 ± 0.10	12.18	F34a (HAe)
3046020669237386624	07034751-1131489	105.9479	-11.5302	0.94 ± 0.06	-4.34 ± 0.13	1.61 ± 0.12	15.95	F05a (WTT)
3046019913323141504	07034869-1131502	105.9529	-11.5306	0.91 ± 0.08	-4.83 ± 0.14	1.33 ± 0.14	16.71	F06 (WTT)
3046019913323142400	07034994-1132148	105.9581	-11.5375	0.85 ± 0.05	-4.37 ± 0.08	1.71 ± 0.07	15.53	F08 (WTT)
3046019604085794560	07035225-1134195	105.9677	-11.5721	0.78 ± 0.10	-4.43 ± 0.20	1.80 ± 0.18	17.04	F11 (WTT)
3046027163227907840	07035414-1128235	105.9756	-11.4732	0.94 ± 0.10	-4.68 ± 0.34	1.33 ± 0.21	16.33	F15 (WTT)
3046027163227906432	07035503-1128181	105.9793	-11.4717	0.83 ± 0.07	-4.69 ± 0.18	1.65 ± 0.15	16.52	F17 (WTT)
3046027163227903104	07035584-1127544	105.9827	-11.4651	0.79 ± 0.06	-4.18 ± 0.10	0.77 ± 0.10	16.30	F21 (WTT)
3046019569726055168	07035587-1133385	105.9828	-11.5607	0.62 ± 0.28	-8.69 ± 0.65	4.87 ± 0.53	15.22	F22 (WTT)
3046027163227905408	07035708-1128317	105.9878	-11.4755	...	-5.47 ± 0.48	3.50 ± 0.42	14.56	F24 (WTT)
3046025548320530304	07035805-1132398	105.9919	-11.5444	0.73 ± 0.08	-4.50 ± 0.15	1.40 ± 0.14	16.70	F25 (WTT)
3045831587598492544	07040114-1136255	106.0047	-11.6071	0.83 ± 0.04	-4.36 ± 0.08	1.64 ± 0.08	15.50	F31 (WTT)
3046027128868163840	07040119-1128454	106.0049	-11.4793	0.73 ± 0.08	-4.29 ± 0.14	1.20 ± 0.13	15.68	F32 (WTT)
3046029121732960384	07040224-1124188	106.0093	-11.4052	0.76 ± 0.07	-4.69 ± 0.12	1.72 ± 0.12	16.27	F33 (WTT?)
3046029117437071616	07040246-1124292	106.0101	-11.4080	0.91 ± 0.09	-4.39 ± 0.17	0.99 ± 0.16	16.47	F35 (WTT)
3046027128868157696	07040309-1128071	106.0129	-11.4686	0.90 ± 0.04	-4.25 ± 0.07	1.60 ± 0.06	15.31	F38 (WTT)
3045837772351358336	07040330-1133586	106.0138	-11.5663	0.86 ± 0.07	-4.33 ± 0.11	1.45 ± 0.12	16.20	F39 (WTT)
3046032076670456064	07040390-1123480	106.0162	-11.3967	0.92 ± 0.06	-4.79 ± 0.10	1.37 ± 0.10	16.31	F36d (WTT)
3046029224812162816	07040725-1123188	106.0303	-11.3886	0.03 ± 0.09	-0.85 ± 0.14	-0.96 ± 0.13	16.71	F44 (WTT)
3046028125300891776	07041601-1126100	106.0667	-11.4361	0.54 ± 0.08	-3.92 ± 0.14	1.41 ± 0.12	15.44	F46 (WTT)
3045837600552637056	07041786-1134268	106.0744	-11.5741	0.63 ± 0.11	-4.25 ± 0.16	1.33 ± 0.16	17.11	F47 (WTT)
3046028159660628352	07041812-1125280	106.0755	-11.4244	0.86 ± 0.04	-4.47 ± 0.07	1.80 ± 0.06	15.39	F48a (WTT)
3046028159660627968	07041839-1125239	106.0766	-11.4233	1.05 ± 0.10	-4.48 ± 0.17	1.75 ± 0.15	16.91	F48b (WTT)
3045836947718876032	07042798-1134431	106.1166	-11.5787	...	-4.21 ± 0.87	-0.95 ± 0.91	14.50	F63 (WTT)

NOTE— Identification and classification of Classical T Tauri (CTT), weak-line T Tauri (WTT), and Herbig Ae (HAe) stars were obtained by Fernandes et al. (2015) based on *GMOS* spectroscopy.

Table 5. New members of CMa R1 identified in the present work. The astrometric data are the same as Table 3 .

Gaia-DR2	2MASS	RA	Dec	P	ϖ	$\mu_\alpha \cos \delta$	μ_δ	G
		degree	degree	%	mas	mas yr ⁻¹	mas yr ⁻¹	mag.
3046062725556787200	00000000-0000000	105.3028	-11.4309	91	0.94±0.10	-3.68±0.15	1.59±0.21	15.69
3046107977332044032	07011780-1107209	105.3242	-11.1225	70	1.10±0.02	-5.02±0.04	1.94±0.04	13.79
3046013792988609408	07012500-1132538	105.3542	-11.5483	84	0.83±0.16	-4.69±0.24	2.05±0.24	18.05
3046064958939721728	07012916-1121307	105.3715	-11.3585	94	0.83±0.05	-3.78±0.09	1.43±0.09	15.90
3046063309672312960	07012943-1125450	105.3726	-11.4292	93	0.92±0.12	-3.75±0.15	1.44±0.18	17.02
.
.
.
3046250295370429824	07063757-1108473	106.6566	-11.1465	57	1.07±0.13	-3.22±0.22	1.83±0.23	17.80
3046145150268232960	07063763-1142490	106.6569	-11.7136	78	0.96±0.28	-3.30±0.38	1.33±0.35	18.23
3046141306281307904	07063777-1146519	106.6574	-11.7811	83	0.98±0.06	-3.65±0.10	1.13±0.10	15.87
3046442018409676416	07063936-1056533	106.6640	-10.9481	72	0.96±0.25	-3.67±0.40	0.77±0.46	18.31
3046245622446043136	07064160-1113590	106.6733	-11.2331	89	0.83±0.04	-3.52±0.07	1.53±0.07	11.96

NOTE— For illustration, only a part of the table is presented. The entire list of objects is available on-line.

Table 6. New candidates (P < 50 percent) identified in the present work. The astrometric data are the same as Table 3.

Gaia-DR2	2MASS	RA	Dec	P	ϖ	$\mu_\alpha \cos \delta$	μ_δ	G
		degree	degree	%	mas	mas yr ⁻¹	mas yr ⁻¹	mag.
3046067364121443840	07011449-1123185	105.3104	-11.3885	25	0.80±0.04	-3.04±0.06	1.05±0.06	14.78
3046092820387743360	07011607-1115513	105.3170	-11.2643	34	0.96±0.28	-3.37±0.50	0.43±0.44	18.78
3046067879517494272	07011974-1121119	105.3323	-11.3533	2	0.86±0.11	-3.34±0.19	0.39±0.20	16.88
3046092515449873024	07012008-1117448	105.3337	-11.2958	27	0.80±0.04	-3.06±0.06	1.05±0.06	14.74
3046091759535625856	07012338-1118004	105.3474	-11.3001	33	0.81±0.04	-3.15±0.08	1.02±0.07	11.94
.
.
.
3046441507311707392	07062918-1058194	106.6216	-10.9720	20	1.06±0.12	-2.81±0.19	1.20±0.21	17.27
3046448821637725952	07063299-1054190	106.6375	-10.9053	3	0.89±0.04	-4.38±0.06	2.53±0.07	12.78
304622223464219392	07063720-1114088	106.6550	-11.2358	11	0.99±0.04	-2.89±0.07	1.82±0.06	14.93
3046206349265151232	07064031-1125376	106.6679	-11.4271	36	1.24±0.10	-4.58±0.15	2.35±0.15	17.02
3045752590258349568	07064328-1154148	106.6804	-11.9041	44	0.94±0.22	-4.20±0.36	0.54±0.35	18.59

NOTE— For illustration, only a part of the table is presented. The entire list of objects is available on-line.

Table 7. Photometric data for *T80S* sources that were previously identified in the literature (see Tables 3 and 4).

ID	u'	m_{378}	m_{395}	m_{410}	m_{430}	g'	m_{515}	r'	m_{660}	i'	m_{861}	z'
W011a	17.04±0.07	17.11±0.08	17.31±0.10	16.90±0.05	16.92±0.05	16.15±0.01	15.95±0.02	15.29±0.01	15.05±0.02	14.79±0.00	14.58±0.01	14.57±0.01
W096	20.24±0.34	20.33±0.89	19.03±0.18	18.31±0.43	17.56±0.11	16.97±0.18	...
W076	20.52±0.52	20.47±0.66	19.81±0.39	20.20±0.36	19.65±0.22	18.84±0.03	18.83±0.09	17.58±0.01	17.25±0.03	16.84±0.01	16.59±0.02	16.59±0.01
W021	18.93±0.18	19.79±0.51	19.66±0.48	18.88±0.15	19.07±0.18	18.13±0.03	17.94±0.06	17.03±0.01	16.73±0.03	16.38±0.01	16.10±0.01	16.10±0.01
W038	19.84±0.27	18.88±0.45	18.17±0.12	17.63±0.32	16.93±0.08	16.47±0.14	...
W047a	...	15.18±0.17	...	14.79±0.07	14.24±0.05	13.75±0.05	13.55±0.04	14.95±0.17	14.44±0.02	13.93±0.02	13.67±0.02	...
W005	...	17.76±0.57	...	17.16±0.22	16.22±0.13	15.40±0.11	14.98±0.07	17.27±0.49	16.45±0.06	15.61±0.04	15.17±0.04	...
W016	...	14.21±0.11	...	14.02±0.05	13.62±0.04	13.35±0.04	13.20±0.03	14.12±0.12	13.78±0.02	13.44±0.01	13.26±0.01	...
S119	20.79±0.68	20.60±0.94	20.84±1.22	20.59±0.51	20.44±0.56	20.24±0.15	20.00±0.32	18.86±0.05	18.39±0.11	17.24±0.02	16.62±0.02	16.49±0.01
C078	20.75±0.60	20.41±0.58	23.58±1.40	22.34±2.37	21.18±0.82	19.46±0.05	19.34±0.13	18.00±0.02	17.58±0.03	16.95±0.01	16.52±0.01	16.45±0.01
W046	17.68±0.06	17.85±0.07	18.09±0.09	17.52±0.05	17.42±0.03	16.75±0.01	16.49±0.01	15.85±0.00	15.62±0.01	15.35±0.00	15.14±0.01	15.13±0.00
S006	13.08±0.00	13.13±0.00	13.41±0.00	13.20±0.00	13.19±0.00	12.98±0.00	12.84±0.00	12.70±0.00	12.63±0.00	12.56±0.00	12.56±0.00	12.60±0.00
S019	18.90±0.15	19.02±0.20	19.29±0.26	18.54±0.10	18.43±0.08	17.69±0.01	17.43±0.03	16.64±0.01	16.39±0.02	16.02±0.01	15.75±0.01	15.72±0.01
[SEI99]52(B8-9)	11.40±0.03	...	11.45±0.03	...	11.27±0.01	11.28±0.01	11.06±0.01	...	11.13±0.02	11.41±0.01	11.08±0.01	...
C041	19.98±0.82	18.80±0.43	16.93±0.23	16.15±0.12	18.80±0.00	18.91±0.17	17.43±0.09	16.50±0.07	...
C042b	20.30±0.34	...	18.79±0.16	17.31±0.27	17.80±0.12	17.23±0.20	...
[SEI99]160(Ae)	11.83±0.00	12.00±0.00	12.08±0.00	12.02±0.00	12.08±0.00	11.93±0.00	11.79±0.00	11.65±0.00	11.37±0.01	11.44±0.00	11.27±0.00	11.23±0.00
C026b	20.45±0.55	20.54±1.03	20.07±0.70	20.41±0.48	20.61±0.76	19.28±0.07	19.34±0.20	17.98±0.03	17.45±0.06	16.96±0.01	16.55±0.02	16.43±0.02
C035	19.63±0.70	18.37±0.35	16.71±0.20	15.84±0.11	18.80±0.00	18.51±0.14	17.08±0.07	16.19±0.06	...
C026a	18.43±0.15	18.97±0.27	18.56±0.19	18.04±0.10	17.99±0.08	17.10±0.01	16.83±0.02	15.96±0.01	15.68±0.01	15.27±0.00	15.02±0.01	14.94±0.01
C001a	11.51±0.00	11.17±0.00	11.22±0.00	10.87±0.00	11.40±0.00	11.31±0.00	11.26±0.00	11.22±0.00	11.14±0.00	11.09±0.00	11.07±0.00	11.08±0.00
C001C	20.05±0.30	...	19.22±0.20	18.77±0.53	17.99±0.13	17.59±0.24	...
C015	18.41±0.39	17.29±0.21	15.90±0.14	15.18±0.08	19.18±1.20	17.40±0.09	16.20±0.05	15.44±0.04	...
C033	19.99±0.42	19.84±0.46	20.89±1.26	19.78±0.31	19.13±0.17	18.19±0.02	18.03±0.05	16.81±0.01	16.43±0.02	15.84±0.01	15.46±0.01	15.33±0.01
C023C ^c	20.17±0.32	20.32±0.89	18.80±0.16	18.42±0.45	17.92±0.12	17.74±0.26	...
C020a	20.41±0.90	21.10±2.77	...	21.09±1.53	19.85±0.60	18.68±0.07	18.74±0.19	17.08±0.02	16.58±0.06	16.10±0.01	15.75±0.02	15.58±0.01
C021b	16.71±0.03	16.95±0.04	17.09±0.05	16.57±0.03	16.57±0.02	15.94±0.00	15.76±0.01	15.18±0.00	14.97±0.01	14.73±0.00	14.58±0.00	14.56±0.00
C017	22.40±3.92	...	23.86±28.44	20.29±0.51	20.76±1.09	19.44±0.11	19.29±0.24	17.72±0.03	17.31±0.08	16.55±0.01	16.10±0.02	15.93±0.01
S002b ^c	18.85±0.94	...	18.11±0.34	17.57±0.09	17.37±0.22	16.63±0.06	16.33±0.17	15.93±0.05	15.69±0.10	...
C044	21.82±1.64	21.42±1.03	20.73±0.86	20.78±0.29	20.03±0.39	18.88±0.06	18.28±0.13	17.45±0.02	17.00±0.03	16.75±0.02
C006	20.52±0.50	21.94±4.19	22.18±5.37	23.06±4.53	22.41±4.37	21.07±0.42	20.18±0.49	19.25±0.09	18.76±0.24	17.86±0.04	17.57±0.06	17.18±0.04
[SEI99]72(B1)	7.36±0.00	7.25±0.00	7.48±0.00	7.67±0.00	7.76±0.00	8.68±0.00	7.86±0.00	9.03±0.00	9.01±0.00	8.95±0.00	8.96±0.00	9.21±0.00
[SEI99]73(B3)	...	10.76±0.02	...	10.84±0.01	10.96±0.01	10.93±0.01	10.81±0.01	10.35±0.02	11.13±0.01	11.97±0.01	22.44±0.00	...
C025	16.51±0.04	16.64±0.04	16.74±0.04	16.32±0.03	16.17±0.02	15.81±0.01	15.76±0.01	14.78±0.00	14.54±0.01	14.09±0.00	14.05±0.00	13.81±0.00
C031	20.26±0.50	20.40±0.78	20.01±0.58	19.34±0.20	19.60±0.26	18.93±0.05	18.67±0.10	17.44±0.01	17.04±0.03	16.24±0.01	16.16±0.01	15.72±0.01
C029	19.42±0.26	19.81±0.44	21.56±2.33	18.87±0.15	18.94±0.14	18.48±0.03	18.22±0.06	16.79±0.01	16.35±0.02	15.52±0.00	15.43±0.01	14.96±0.00
C097	19.77±0.26	20.16±0.49	...	19.72±0.23	19.87±0.26	19.24±0.05	18.94±0.10	17.76±0.01	17.28±0.03	16.52±0.01	16.44±0.01	15.91±0.01

Table 7 continued

Table 7 (continued)

ID	u'	m378	m395	m410	m430	g'	m515	r'	m660	i'	m861	z'
[SEI99]77(B3)	11.56±0.01	11.83±0.01	11.95±0.01	11.83±0.01	11.86±0.01	12.08±0.00	11.98±0.01	11.72±0.00	11.64±0.02	11.52±0.01	11.58±0.01	11.51±0.01
C067	20.20±0.49	20.03±0.97	20.39±0.87	20.35±0.28	...	18.71±0.08	17.86±0.15	17.53±0.04	17.42±0.07	16.88±0.04
C059	23.23±6.40	...	18.87±0.46	25.02±29.76	21.44±3.36	19.36±0.23	18.42±0.48	17.57±0.06	17.23±0.10	16.58±0.05
C032	19.42±0.26	20.13±0.60	19.80±0.45	19.57±0.27	19.09±0.16	18.44±0.03	18.52±0.08	16.77±0.01	16.41±0.02	15.71±0.00	15.60±0.01	15.22±0.00
C071	13.92±0.01	14.51±0.01	15.26±0.02	14.90±0.01	14.86±0.01	14.28±0.00	14.63±0.01	14.04±0.00	14.39±0.01	13.86±0.00	14.38±0.01	13.66±0.00
E076a	20.96±0.81	20.56±0.76	20.26±0.61	19.93±0.29	19.80±0.27	19.02±0.04	18.84±0.10	17.70±0.01	17.40±0.03	16.86±0.01	16.59±0.02	16.42±0.01
[SEI99]82(B8)	...	13.71±0.09	...	13.66±0.04	13.69±0.04	13.78±0.05	13.99±0.05	12.61±0.06	13.00±0.01	13.04±0.01	13.09±0.01	...
C057	18.80±0.15	19.12±0.44	19.71±0.63	19.98±0.40	19.22±0.27	18.60±0.05	19.85±0.41	17.80±0.03	18.44±0.23	17.34±0.03	18.33±0.14	17.18±0.04
[SEI99]84(A)	...	14.31±0.12	...	13.80±0.05	13.71±0.04	13.50±0.05	13.50±0.04	13.62±0.09	13.65±0.01	13.52±0.01	13.29±0.01	...
E077	19.13±1.17	18.54±0.15	19.44±0.58	17.63±0.10	18.45±0.46	16.99±0.08	17.99±0.29	...
E173	19.36±0.21	20.21±0.84	18.22±0.12	18.93±0.57	17.41±0.10	18.38±0.34	...
C051a	20.43±1.03	18.78±0.16	19.57±0.62	17.55±0.09	18.16±0.40	16.68±0.07	17.46±0.23	...
E039	19.69±0.25	...	18.47±0.14	19.03±0.60	17.52±0.10	18.09±0.30	...
E142	20.29±0.57	19.83±0.43	20.37±0.72	19.27±0.19	19.08±0.15	18.43±0.03	18.52±0.08	16.99±0.01	16.68±0.02	15.86±0.00	15.82±0.01	15.32±0.01
F13(CTT)	...	18.89±0.96	...	18.32±0.38	17.64±0.25	16.56±0.19	16.47±0.14	16.97±0.43	16.79±0.07	15.95±0.04	15.40±0.04	...
E107a	19.23±0.20	19.01±0.60	18.23±0.14	18.28±0.33	...
E107b	19.12±0.55	18.19±0.12	18.44±0.36	16.94±0.07	16.98±0.23	16.23±0.06	16.51±0.14	...
F14(CTT)	...	18.72±0.89	...	18.07±0.34	17.31±0.21	16.30±0.17	16.01±0.12	17.16±0.47	16.61±0.06	15.72±0.04	15.14±0.04	...
E015b	18.79±0.16	18.79±0.54	17.73±0.12	18.56±0.38	...
E074	19.47±0.23	19.88±0.71	18.25±0.13	18.18±0.41	17.35±0.10	17.45±0.22	...
E015a	19.62±0.24	...	18.38±0.14	19.02±0.60	17.55±0.11	18.32±0.34	...
E079	20.21±0.44	19.85±0.42	20.79±1.06	20.88±0.75	20.25±0.43	19.15±0.05	19.00±0.13	17.75±0.02	17.50±0.04	16.68±0.01	16.67±0.02	16.08±0.01
E031C	21.40±0.86	20.19±1.17	22.30±8.24	...	21.25±2.13	...	20.34±0.80	19.88±0.25	...	18.12±0.07	17.64±0.10	17.44±0.07
F20a(WTT)	...	19.00±0.00	...	19.79±0.75	18.87±0.44	17.68±0.32	17.18±0.20	18.97±1.09	17.95±0.11	16.92±0.07	16.19±0.06	...
C047b	20.45±0.36	...	19.20±0.20	19.60±0.79	17.78±0.12	18.60±0.38	...
E378a	20.49±0.37	...	19.00±0.18	19.55±0.77	17.77±0.12	18.65±0.39	...
E099	19.18±0.20	19.25±0.53	17.62±0.10	17.65±0.32	16.53±0.07	16.79±0.17	...
E042	...	16.45±0.31	...	15.94±0.12	15.42±0.09	14.84±0.09	14.67±0.06	14.87±0.16	14.88±0.03	14.37±0.02	13.98±0.02	...
E078	...	19.00±0.00	...	19.41±0.63	18.37±0.35	17.44±0.29	17.12±0.19	18.40±0.84	17.60±0.09	16.65±0.06	16.07±0.05	...
F27(WTT)	9.98±0.00	8.51±0.00	9.09±0.00	10.42±0.01	9.21±0.00	10.45±0.02	9.33±0.00	10.60±0.00	9.99±0.02	10.54±0.00	9.67±0.00	10.38±0.01
[SEI99]101(B6-8)	...	19.00±0.00	...	20.45±0.00	20.65±0.00	20.15±0.00	20.70±0.00	18.80±0.00	22.74±0.00	22.75±0.00	22.44±0.00	...
E085	...	18.78±0.91	...	18.24±0.36	17.75±0.26	17.22±0.26	17.02±0.18	16.86±0.41	16.96±0.07	16.41±0.05	16.00±0.05	...
E086b	...	14.73±0.14	...	14.61±0.07	14.59±0.06	14.51±0.07	14.69±0.06	13.68±0.10	13.79±0.02	13.74±0.02	13.86±0.02	...
F40(B3-5)	...	13.00±0.06	...	13.05±0.03	13.20±0.03	13.33±0.04	13.59±0.04	11.19±0.03	12.35±0.01	12.50±0.01	12.46±0.01	...
[SEI99]100(B8-9)	...	13.67±0.09	...	13.70±0.04	13.78±0.04	13.80±0.05	14.00±0.05	12.54±0.06	12.95±0.01	12.97±0.01	12.89±0.01	...
E019b	20.70±0.41	...	18.65±0.15	18.86±0.56	17.21±0.09	17.38±0.22	...
E075	18.91±1.06	19.91±0.80	18.07±0.12	18.93±0.46	17.09±0.07	17.85±0.35	16.45±0.06	17.45±0.23	...
E019a	18.57±0.15	19.14±0.51	17.37±0.08	17.66±0.32	16.53±0.07	17.00±0.18	...
E043b	19.23±0.20	19.84±0.70	17.98±0.11	18.09±0.39	17.15±0.09	17.43±0.22	...

Table 7 continued

Table 7 (continued)

ID	u'	m_{378}	m_{395}	m_{410}	m_{430}	g'	m_{515}	r'	m_{660}	i'	m_{861}	z'
[SEI99]102	9.71±0.00	10.61±0.00	11.02±0.00	11.11±0.00	11.17±0.00	10.86±0.00	11.28±0.00	11.04±0.00	11.31±0.01	11.11±0.00	11.68±0.00	11.11±0.00
E127	17.98±0.08	18.20±0.11	18.10±0.10	17.64±0.06	17.56±0.04	16.91±0.01	16.77±0.02	16.02±0.00	15.80±0.01	15.50±0.00	15.34±0.01	15.28±0.01
[SEI99]162(B5e)	...	14.16±0.11	...	14.18±0.06	14.18±0.05	13.71±0.05	14.12±0.05	12.69±0.06	13.41±0.01	13.30±0.01	13.12±0.01	...
E140a	20.37±0.91	18.93±0.17	18.45±0.46	17.71±0.11	17.60±0.24	...
E014a	21.33±0.57	...	20.53±0.38	19.94±0.93	19.15±0.22	18.94±0.45	...
E096	21.20±0.84	...	21.04±1.09	21.33±0.86	23.01±4.40	19.89±0.08	19.76±0.19	18.44±0.02	17.96±0.05	17.29±0.01	16.88±0.02	16.80±0.01
E113b	19.05±0.18	19.32±0.55	17.73±0.10	17.32±0.27	16.59±0.07	16.48±0.14	...
E020a	18.55±0.15	19.45±0.58	17.59±0.09	18.26±0.42	16.94±0.08	17.79±0.26	...
E081	20.84±0.44	20.87±1.16	19.28±0.21	19.47±0.74	18.15±0.14	18.58±0.38	...
E038	17.28±0.06	17.36±0.07	18.33±0.18	17.24±0.06	16.77±0.03	16.48±0.01	16.25±0.02	15.48±0.00	15.09±0.01	14.55±0.00	14.49±0.00	13.83±0.00
[SEI99]108(B6-8)	...	19.00±0.00	...	20.45±0.00	20.65±0.00	20.15±0.00	20.70±0.00	18.80±0.00	22.74±0.00	22.75±0.00	22.44±0.00	...
[SEI99]111(B8)	10.29±0.01	10.11±0.01	10.10±0.01	10.60±0.01	9.96±0.00	10.29±0.00	9.80±0.00	10.20±0.01	10.87±0.09	9.93±0.01	9.65±0.01	9.98±0.01
E108	19.02±0.62	17.82±0.21	17.17±0.27	17.61±0.18	18.67±1.00	16.30±0.09	16.13±0.49	15.25±0.05	15.29±0.10	14.54±0.04
E154	19.69±0.25	19.64±0.64	18.38±0.14	18.02±0.38	17.38±0.10	17.23±0.20	...
E129	19.35±0.21	19.19±0.52	17.79±0.10	17.27±0.27	16.38±0.06	16.04±0.12	...
E205b	19.72±0.30	20.50±1.04	20.42±1.01	20.50±0.57	20.44±0.68	19.19±0.07	19.00±0.16	17.91±0.03	17.35±0.06	16.78±0.01	16.59±0.02	15.98±0.01
E205a	20.94±0.81	19.96±0.75	19.78±0.65	20.88±0.69	19.99±0.52	20.10±0.19	...	19.19±0.10	18.44±0.21	18.02±0.05	17.97±0.10	17.39±0.05
E111b	20.94±0.47	...	19.51±0.23	19.66±0.81	18.01±0.13	18.28±0.33	...
E087a	...	22.44±4.07	19.92±0.09	20.18±0.30	18.55±0.03	18.55±0.10	17.53±0.02	17.54±0.04	16.98±0.02
E177	...	14.81±0.15	...	14.58±0.07	14.40±0.06	14.25±0.07	14.23±0.05	13.86±0.10	13.73±0.02	13.62±0.01	13.43±0.02	...
E120a	19.43±0.33	...	20.49±1.79	21.46±1.94	19.54±0.51	19.00±0.11	20.05±0.71	17.55±0.04	17.80±0.21	16.76±0.02	17.30±0.08	16.31±0.03
E120b	21.78±1.06	20.55±0.98	...	24.32±7.24	21.61±0.66	20.71±1.11	19.19±0.10	19.35±0.25	18.41±0.09
[SEI99]116(A1)	13.05±0.00	12.99±0.01	12.61±0.00	12.44±0.00	12.47±0.00	12.58±0.00	12.58±0.00	12.09±0.00	11.93±0.00	11.73±0.00	11.84±0.00	11.61±0.00
E141a	21.12±1.11	18.95±0.56	21.54±6.06	...	19.83±0.85	20.16±0.42	...	19.11±0.21	20.50±3.79	17.96±0.10	17.77±0.18	17.24±0.09
E141b	21.74±1.79	18.68±0.45	20.17±1.73	20.85±0.89	18.74±0.32	20.72±0.72	...	20.18±0.58	20.35±3.37	18.52±0.18	18.44±0.33	17.92±0.18
E030a	19.01±1.11	19.17±0.56	17.90±0.11	18.17±0.32	16.93±0.07	16.95±0.23	16.20±0.06	16.40±0.14	...
E030b	19.84±0.27	20.16±0.82	18.51±0.14	18.41±0.45	17.59±0.11	17.70±0.25	...
E105	20.31±0.38	19.72±0.43	...	21.84±1.37	20.38±0.53	19.94±0.11	19.61±0.23	18.63±0.05	17.99±0.09	17.43±0.02	17.25±0.03	16.86±0.02
F50(WTT)	18.74±0.17	19.51±0.41	20.19±0.79	18.82±0.16	18.69±0.13	17.74±0.02	17.70±0.05	16.59±0.01	16.42±0.02	15.71±0.01	15.67±0.01	15.13±0.01
[SEI99]117(A0)	12.49±0.01	12.36±0.01	12.10±0.01	12.12±0.01	12.18±0.00	12.14±0.00	12.23±0.00	12.00±0.00	11.86±0.02	11.96±0.00	12.02±0.01	11.97±0.01
E004	...	18.67±0.86	...	17.87±0.31	17.17±0.20	16.26±0.17	15.89±0.11	17.56±0.57	17.03±0.07	16.27±0.05	15.71±0.04	...
E128	20.23±0.62	20.52±1.51	...	20.43±0.68	21.04±1.66	18.90±0.08	19.30±0.30	17.57±0.03	17.28±0.10	16.70±0.02	16.38±0.03	16.30±0.02
E122	20.31±0.34	...	18.73±0.16	18.48±0.47	17.51±0.10	17.46±0.23	...
E071	20.54±0.38	...	19.02±0.18	18.56±0.48	17.64±0.11	17.49±0.23	...
E033	21.16±0.86	20.06±0.45	20.42±0.66	22.82±3.40	20.87±0.66	19.89±0.08	19.59±0.17	18.23±0.02	17.65±0.04	17.02±0.01	16.84±0.02	16.40±0.01
E143	18.86±0.26	19.31±0.85	19.01±0.26	20.11±1.62	17.86±0.13	17.49±0.51	17.19±0.10	17.41±0.24	16.81±0.12
E007b	21.34±0.57	...	19.64±0.24	19.05±0.61	17.80±0.12	17.58±0.24	...
E007a	16.92±0.06	16.91±0.06	17.21±0.09	16.38±0.04	16.32±0.03	15.84±0.01	15.64±0.01	14.87±0.00	14.61±0.01	14.13±0.00	14.15±0.01	13.80±0.00
E126	19.09±0.19	19.08±0.49	17.61±0.09	17.27±0.27	16.65±0.07	16.47±0.14	...

Table 7 continued

Table 7 (continued)

ID	u'	m378	m395	m410	m430	g'	m515	r'	m660	i'	m861	z'
[SEI99]119(B5)	...	10.85±0.02	...	10.88±0.01	11.08±0.01	11.08±0.01	11.23±0.01	10.52±0.02	11.29±0.01	22.75±0.00	11.47±0.01	...
E013	...	19.00±0.00	...	18.45±0.40	17.71±0.26	16.41±0.18	15.83±0.11	18.79±1.00	17.59±0.09	16.52±0.06	15.76±0.05	...
E049	...	19.21±1.11	...	18.96±0.51	17.94±0.29	16.63±0.20	16.02±0.12	18.94±1.07	17.79±0.10	16.72±0.06	15.92±0.05	...
E047	...	19.00±0.00	...	18.95±0.51	18.20±0.33	16.73±0.21	16.23±0.13	18.80±0.00	18.36±0.13	17.21±0.08	16.27±0.06	...
F55(CTT)	...	19.00±0.00	...	18.55±0.42	17.55±0.24	16.20±0.16	15.61±0.10	18.99±1.10	17.61±0.09	16.46±0.06	15.61±0.04	...
E018b	21.48±1.38	21.63±3.04	...	21.27±1.03	20.72±0.91	19.93±0.15	19.57±0.27	18.42±0.04	17.82±0.09	17.09±0.02	16.90±0.03	16.37±0.02
[SEI99]123(B5-7)	11.13±0.01	11.27±0.01	11.52±0.01	11.41±0.01	11.52±0.01	11.56±0.00	11.43±0.00	11.34±0.00	11.01±0.02	10.89±0.00	10.65±0.01	10.41±0.00
E035b	...	19.00±0.00	...	19.36±0.61	18.26±0.34	16.66±0.20	16.09±0.12	18.80±0.00	18.44±0.14	17.20±0.08	16.19±0.06	...
E035a	20.94±0.47	...	20.01±0.29	18.82±0.55	18.22±0.14	17.82±0.27	...
E098a	...	19.00±0.00	...	19.68±0.71	18.93±0.46	17.01±0.24	15.98±0.11	18.80±0.00	19.08±0.19	17.63±0.10	16.18±0.06	...
F72(CTT)	...	20.75±1.74	...	21.11±1.01	20.41±0.85	19.43±0.12	19.81±0.43	17.90±0.03	17.37±0.09	16.74±0.02	16.36±0.03	16.09±0.02
E203	19.69±0.25	19.70±0.66	18.24±0.13	17.66±0.32	16.81±0.07	16.64±0.15	...
E112	20.27±0.95	19.40±0.22	19.31±0.55	17.87±0.11	17.41±0.28	16.70±0.07	16.49±0.14	...
E132	...	15.41±0.19	...	14.64±0.07	14.29±0.05	13.42±0.04	13.16±0.03	14.98±0.17	14.43±0.02	13.75±0.02	13.11±0.01	...
E100	20.75±0.50	21.09±0.92	20.18±0.42	20.81±0.47	23.98±0.04	20.95±0.17	20.84±0.43	19.16±0.04	18.57±0.06	17.51±0.01	17.10±0.02	16.85±0.01
E041a	19.83±0.27	19.85±0.71	18.36±0.13	17.95±0.36	17.30±0.09	17.03±0.18	...
E041b	...	17.89±0.60	...	17.24±0.23	16.52±0.15	15.51±0.12	15.05±0.07	17.66±0.59	16.67±0.06	15.73±0.04	15.16±0.04	...
E135	...	17.87±0.59	...	17.11±0.21	16.62±0.16	15.56±0.12	15.21±0.08	17.63±0.58	16.76±0.06	15.86±0.04	15.16±0.04	...
[SEI99]131	13.94±0.01	13.84±0.01	13.84±0.01	13.80±0.01	13.84±0.00	13.59±0.00	13.43±0.00	13.16±0.00	13.07±0.00	12.85±0.00	12.72±0.00	12.69±0.00
[SEI99]129	13.65±0.01	13.50±0.00	13.44±0.00	13.36±0.00	13.43±0.00	13.28±0.00	13.16±0.00	13.09±0.00	13.04±0.00	12.95±0.00	12.91±0.00	12.90±0.00
[SEI99]132(B6-7)	11.52±0.00	11.52±0.00	11.58±0.00	11.61±0.00	11.73±0.00	11.70±0.00	11.69±0.00	11.77±0.00	11.80±0.00	11.83±0.00	11.93±0.00	11.94±0.00
E070	13.02±0.03	9.71±0.00	9.93±0.00	13.32±0.04	9.34±0.00	11.72±0.00	10.49±0.00	11.74±0.01	11.34±0.03	11.63±0.01	10.59±0.01	11.27±0.01
E021	...	14.62±0.13	...	14.16±0.06	13.67±0.04	12.93±0.04	12.66±0.03	14.43±0.13	13.78±0.02	13.11±0.01	12.70±0.01	...
E029a	17.98±0.10	18.07±0.16	18.01±0.15	18.00±0.10	17.79±0.08	17.22±0.02	16.97±0.04	16.43±0.01	16.16±0.04	15.97±0.01	15.85±0.02	15.80±0.01
E124	21.61±1.56	20.50±0.71	19.42±0.28	19.95±0.35	19.90±0.29	18.65±0.03	18.63±0.08	17.23±0.01	16.88±0.02	16.26±0.01	15.94±0.01	15.79±0.01
E045	15.74±0.02	17.20±0.05	17.48±0.07	17.07±0.04	17.00±0.03	15.84±0.00	16.02±0.01	15.06±0.00	14.91±0.01	14.53±0.00	14.38±0.00	14.29±0.00
E001	16.66±0.04	16.83±0.04	16.91±0.04	16.49±0.03	16.29±0.02	15.51±0.00	15.31±0.01	14.54±0.00	14.28±0.00	13.96±0.00	13.74±0.00	13.71±0.00
E151	14.39±0.01	14.27±0.01	14.39±0.01	14.22±0.01	14.22±0.00	13.99±0.00	13.83±0.00	13.67±0.00	13.58±0.00	13.49±0.00	13.45±0.00	13.48±0.00
E054	18.40±0.15	18.33±0.14	18.40±0.15	17.83±0.08	17.53±0.05	16.50±0.01	16.41±0.02	15.22±0.00	14.89±0.01	14.42±0.00	14.13±0.00	14.04±0.00
E202a	13.24±0.00	13.10±0.00	13.00±0.00	12.90±0.00	12.96±0.00	12.84±0.00	12.75±0.00	12.74±0.00	12.74±0.00	12.67±0.00	12.69±0.00	12.70±0.00
E121	19.75±0.33	19.41±0.29	20.44±0.79	19.04±0.16	18.77±0.11	17.82±0.02	17.67±0.04	16.51±0.01	16.16±0.01	15.72±0.00	15.41±0.01	15.37±0.01
E134	13.42±0.00	13.28±0.00	13.16±0.00	13.04±0.00	13.12±0.00	12.98±0.00	12.89±0.00	12.85±0.00	12.84±0.00	12.75±0.00	12.76±0.00	12.76±0.00
E073	16.88±0.04	17.02±0.05	17.13±0.05	16.55±0.03	16.37±0.02	15.64±0.00	15.44±0.01	14.70±0.00	14.46±0.00	14.20±0.00	14.03±0.00	14.00±0.00
[SEI99]144(B5V)	8.82±0.00	8.79±0.00	8.96±0.00	9.19±0.00	9.19±0.00	9.98±0.00	9.25±0.00	10.22±0.00	9.73±0.00	10.59±0.00	9.72±0.00	10.06±0.00
F10b(CTT)	18.19±0.12	19.12±0.55	18.44±0.36	16.94±0.07	16.98±0.23	16.23±0.06	16.51±0.15
F18(CTT?)	19.21±0.52	17.54±0.09	17.57±0.31	16.50±0.07	16.57±0.15	...
F23(CTT)	19.19±0.20	19.25±0.53	17.63±0.10	17.65±0.32	16.53±0.07	16.79±0.17
F30(CTT)	18.38±0.14	18.98±0.47	17.04±0.07	17.22±0.26	15.92±0.05	16.29±0.13	...
F36c(CTT)	19.52±0.23	19.60±0.79	18.11±0.14	17.90±0.28	...

Table 7 continued

Table 7 (*continued*)

ID	u'	m378	m395	m410	m430	g'	m515	r'	m660	i'	m861	z'
F37(CTT)	19.49±0.23	...	18.07±0.12	18.46±0.46	17.06±0.08	17.74±0.26	...
F60(CTT)
F34a(HAe)	13.68±0.10	...	14.73±0.14	...	14.62±0.07	13.79±0.02	14.60±0.06	13.74±0.02	14.51±0.08	13.86±0.02	14.69±0.06	...
F05a(WTT)	20.43±1.03	18.78±0.16	19.57±0.62	17.56±0.09	18.16±0.40	16.68±0.07	17.46±0.23	...
F06(WTT)	19.69±0.25	...	18.47±0.14	19.03±0.60	17.52±0.10	18.09±0.30	...
F08(WTT)	18.20±0.76	...	19.28±1.15	...	19.17±0.56	17.65±0.10	18.51±0.38	16.89±0.07	17.62±0.31	16.35±0.06	17.24±0.20	...
F11(WTT)	20.07±0.30	...	18.47±0.14	18.70±0.52	17.48±0.10	17.89±0.28	...
F15(WTT)	18.79±0.16	18.79±0.54	17.73±0.12	18.57±0.38	...
F17(WTT)	19.62±0.24	...	18.39±0.14	19.02±0.60	17.55±0.11	18.32±0.34	...
F20a(WTT)	18.97±1.09	19.79±0.75	17.95±0.11	18.87±0.44	17.68±0.07	17.68±0.32	16.19±0.06	17.18±0.20	...
F21(WTT)	19.06±0.19	20.11±0.80	18.03±0.12	18.80±0.54	17.32±0.10	18.33±0.34	...
F22(WTT)	17.89±0.11	18.55±0.38	16.57±0.06	17.06±0.24	15.64±0.04	16.23±0.13	...
F24(WTT)	18.11±0.73	19.02±0.52	17.33±0.08	18.22±0.33	16.33±0.05	17.08±0.24	15.62±0.04	16.57±0.15	...
F25(WTT)	19.47±0.23	...	18.15±0.12	18.53±0.48	17.18±0.09	17.90±0.28	...
F31(WTT)	18.67±0.44	17.68±0.10	17.74±0.26	16.63±0.06	16.56±0.19	15.86±0.05	16.04±0.12	...
F32(WTT)	18.41±0.14	19.52±0.60	17.44±0.09	18.20±0.41	16.72±0.07	17.68±0.25	...
F33(WTT?)	19.71±0.25	...	18.24±0.13	18.41±0.45	17.05±0.08	17.42±0.22	...
F35(WTT)	19.56±0.24	...	18.30±0.13	18.54±0.48	17.29±0.09	17.74±0.26	...
F38(WTT)	18.91±1.06	19.91±0.80	18.07±0.12	18.93±0.46	17.09±0.07	17.85±0.35	16.45±0.06	17.46±0.23	...
F39(WTT)	18.57±0.15	19.14±0.51	17.37±0.08	17.67±0.32	16.53±0.07	17.00±0.18	...
F44(WTT)	19.81±0.27	...	18.43±0.14	18.39±0.45	17.44±0.10	17.44±0.22	...
F46(WTT)	19.58±1.32	...	19.21±0.57	17.95±0.11	18.25±0.33	16.91±0.07	17.07±0.24	16.09±0.05	16.45±0.14	...
F47(WTT)	20.15±0.31	...	18.63±0.15	18.18±0.40	17.12±0.09	16.91±0.18	...
F48a(WTT)	19.01±1.11	19.17±0.56	17.90±0.11	18.17±0.32	16.93±0.07	16.95±0.23	16.20±0.06	16.40±0.14	...
F48b(WTT)	19.84±0.27	20.16±0.82	18.51±0.14	18.41±0.45	17.59±0.11	17.70±0.25	...
F63(WTT)	17.45±0.54	...	17.96±0.62	...	16.92±0.20	16.29±0.05	16.12±0.12	15.23±0.03	14.87±0.09	14.34±0.02	14.31±0.05	...

NOTE— The error bars denoted by 0.00 represent magnitude errors lower than 0.01 mag. The *T80S* sources are the same ones appearing in Table 2.

Table 8. Photometric data for *T80S* sources that are suggested to be new members of CMa R1, identified in the present work (see Table 5)

Gaia-DR2	u'	m_{378}	m_{395}	m_{410}	m_{430}	g'	m_{515}	γ'	m_{660}	i'	m_{861}	z'
3046062725556787200	17.62±0.07	17.63±0.07	17.88±0.10	17.30±0.05	17.07±0.03	16.31±0.01	16.06±0.01	15.31±0.00	15.08±0.01	14.81±0.00	14.60±0.00	14.60±0.00
304610797332044032	14.36±0.01	14.54±0.01	14.86±0.01	14.49±0.01	14.46±0.01	14.07±0.00	13.87±0.00	13.57±0.00	13.44±0.00	13.36±0.00	13.29±0.00	13.34±0.00
3046013792988609408	21.49±1.12	20.58±0.68	20.23±0.53	22.04±1.66	21.12±0.76	19.91±0.08	19.77±0.19	18.50±0.02	18.05±0.05	17.45±0.01	17.03±0.02	17.00±0.02
3046064958939721728	17.60±0.08	17.51±0.09	18.03±0.15	17.49±0.07	17.41±0.06	16.77±0.01	16.36±0.02	15.97±0.01	15.75±0.02	15.54±0.01	15.36±0.01	15.35±0.01
304606330967231296	19.66±0.28	18.98±0.19	19.16±0.24	20.33±0.48	19.23±0.17	18.44±0.03	18.26±0.06	17.15±0.01	16.83±0.02	16.44±0.01	16.11±0.01	16.10±0.01
.
.
.
3046250295370429824	19.83±0.39	19.60±0.37	...	19.82±0.28	19.52±0.24	19.43±0.07	19.18±0.14	18.10±0.03	17.42±0.04	17.15±0.01	16.74±0.02	16.70±0.02
3046145150268232960	20.31±0.50	19.62±0.39	19.33±0.33	20.23±0.42	19.51±0.24	19.28±0.06	18.94±0.12	18.37±0.03	18.15±0.08	17.90±0.03	17.69±0.05	17.67±0.04
3046141306281307904	17.14±0.05	17.25±0.07	17.42±0.08	17.08±0.05	17.03±0.04	16.56±0.01	16.33±0.02	15.88±0.01	15.69±0.02	15.53±0.01	15.40±0.01	15.44±0.01
3046442018409676416	21.05±1.40	19.70±0.53	22.34±6.69	21.06±1.21	21.11±1.25	20.68±0.25	20.49±0.58	18.95±0.06	18.48±0.11	17.58±0.03	17.13±0.03	17.03±0.03
3046245622446043136	11.95±0.40	11.97±0.00	11.90±0.00	11.97±0.00	12.05±0.00	12.03±0.00	11.97±0.00	12.07±0.00	12.09±0.00	12.12±0.00	12.18±0.00	12.22±0.00

NOTE— The error bars denoted by 0.00 represent magnitude errors lower than 0.01 mag. For illustration, only a part of the table is presented. The entire list of objects is available on-line.

Table 9. Photometric data for *T80S* sources identified in the present work as candidates that we suggested to be possible members of CMa R1 (see Table 6)

Gaia-DR2	u'	m_{378}	m_{395}	m_{410}	m_{430}	g'	m_{515}	γ'	m_{660}	i'	m_{861}	z'
304606736412144384	16.12±0.02	16.13±0.02	16.32±0.03	16.07±0.02	16.00±0.01	15.56±0.00	15.32±0.01	14.85±0.00	14.69±0.01	14.46±0.00	14.28±0.00	14.28±0.00
3046092820387743360	22.07±2.25	22.84±9.61	20.40±1.07	...	19.78±0.39	20.57±0.26	19.61±0.29	19.19±0.09	18.82±0.25	17.96±0.04	17.45±0.05	17.37±0.04
3046067879517494272	18.47±0.10	18.42±0.11	18.44±0.12	18.47±0.09	18.51±0.09	17.90±0.02	17.59±0.03	17.04±0.01	16.84±0.02	16.54±0.01	16.31±0.01	16.30±0.01
3046092515449873024	15.99±0.02	15.92±0.02	15.99±0.02	15.81±0.02	15.76±0.01	15.40±0.00	15.16±0.01	14.82±0.00	14.69±0.01	14.49±0.00	14.34±0.00	14.35±0.00
3046091759535625856	12.52±0.00	12.43±0.00	12.47±0.00	12.51±0.00	12.52±0.00	12.35±0.00	12.19±0.00	12.00±0.00	11.92±0.00	11.82±0.00	11.72±0.00	11.72±0.00
.
.
.
3046441507311707392	20.08±0.39	...	19.47±0.32	20.08±0.34	20.59±0.53	18.97±0.04	19.02±0.11	17.59±0.01	17.23±0.03	16.74±0.01	16.43±0.01	16.39±0.01
3046448821637725952	13.46±0.01	13.39±0.00	13.46±0.01	13.32±0.00	13.33±0.00	13.12±0.00	12.98±0.00	12.83±0.00	12.77±0.00	12.68±0.00	12.64±0.00	12.68±0.00
304622223464219392	15.91±0.02	16.06±0.03	16.36±0.03	15.92±0.02	15.96±0.02	15.50±0.00	15.31±0.01	14.96±0.00	14.81±0.01	14.71±0.00	14.61±0.01	14.66±0.00
3046206349265151232	20.38±0.85	...	22.05±5.79	19.48±0.32	19.99±0.54	18.60±0.05	18.70±0.14	17.27±0.02	16.89±0.04	16.42±0.01	16.09±0.02	16.09±0.01
3045752590258349568	21.18±1.35	20.86±0.89	20.44±0.61	20.47±0.19	19.97±0.33	19.15±0.06	18.51±0.10	17.83±0.03	17.38±0.04	17.37±0.03

NOTE— The error bars denoted by 0.00 represent magnitude errors lower than 0.01 mag. For illustration, only a part of the table is presented. The entire list of objects is available on-line.

ACKNOWLEDGMENTS

This work was partially supported by FAPESP Proc. 2014/18100-4 (JGH), Proc. 2017/18191-8 (FN), Proc. 2017/19458-8 (AH), Proc. 2018/06822-6 (TSS), Proc. 2018/21250-9 (HDP), Proc. 2018/05866-0 (VJP). JGH acknowledges support from CNPq (305590/2016-6). We thank Stavros Akras, Fábio R. Herpich, and Alvaro Alvarez-Candal for their suggestions and comments on the manuscript.

This work has made use of data from the European Space Agency (ESA) mission *Gaia* (<https://www.cosmos.esa.int/gaia>), processed by the *Gaia* Data Processing and Analysis Consortium (DPAC, <https://www.cosmos.esa.int/web/gaia/dpac/consortium>). Funding for the DPAC has been provided by national institutions, in particular the institutions participating in the *Gaia* Multilateral Agreement.

The S-PLUS project, including the T80-South robotic telescope and the S-PLUS scientific survey, was founded as a partnership between the Fundação de Amparo à Pesquisa do Estado de São Paulo (FAPESP), the Observatório Nacional (ON), the Federal University of Sergipe (UFS), and the Federal University of Santa Catarina

(UFSC), with important financial and practical contributions from other collaborating institutes in Brazil, Chile (Universidad de La Serena), and Spain (Centro de Estudios de Física del Cosmos de Aragón, CEFCA). We further acknowledge financial support from the São Paulo Research Foundation (FAPESP), the Brazilian National Research Council (CNPq), the Coordination for the Improvement of Higher Education Personnel (CAPES), the Carlos Chagas Filho Rio de Janeiro State Research Foundation (FAPERJ), and the Brazilian Innovation Agency (FINEP).

The authors who are members of the S-PLUS collaboration are grateful for the contributions from CTIO staff in helping in the construction, commissioning and maintenance of the T80-South telescope and camera. We are also indebted to Rene Laporte and INPE, as well as Keith Taylor, for their important contributions to the project. From CEFCA, we thank Antonio Marín-Franch for his invaluable contributions in the early phases of the project, David Cristóbal-Hornillos and his team for their help with the installation of the data reduction package JYPE version 0.9.9, César Íñiguez for providing 2D measurements of the filter transmissions, and all other staff members for their support with various aspects of the project.

REFERENCES

- André, Ph., Men'shchikov, A., Bontemps, S. et al. 2010, *A&A*, 518, 102
- Bessell, M. S., 1990, *PASP*, 102, 1181
- Bertin, E. 2010, SWarp: Resampling and Co-adding FITS Images Together, Astrophysics Source Code Library (ascl:1010.068)
- Bertin E., Arnouts S., 1996, *A&A*, 117, 393
- Bonatto, C. 2019, *MNRAS*, 483, 2758
- Brand, J., Massi, F., Zavagno, A., Deharveng, L., Lefloch, B. 2011, *A&A*, 527, 62
- Bressan, A., Marigo, P., Girardi, L., Salasnich, B., Dal Cero, C., Rubele, S., Nanni, A., 2012, *MNRAS*, 427, 127
- Briceño, C., Calvet, N., Hernández, J. et al. 2019, *AJ*, 157, 85
- Cenarro, A. J., et al. 2019, *A&A*, 622, A176
- Christiaens, V.; Cantalloube, F.; Casassus, S.; Price, D.J.; Absil, O.; Pinte, C.; Girard, J.; Montesinos, M., 2019, *ApJ*, 877, L33
- Claría, J. J., 1974, *AJ*, 79, 1022
- Cloutier, R., Currie, T., Rieke, G. H., et al. 2014, *ApJ*, 796, 127
- Cohen, M., Kuhl, L. V. 1979 *ApJS* 41, 743
- Covey, K. R., Ivezić, Ž., Schlegel, D. et al. 2007, *AJ*, 134, 2398
- Diolaiti, E., Bendinelli, O., Bonaccini, D., Close, L., Currie, D., Parmeggiani, G., 2000, *A&AS*, 147, 335
- Donati, J.-F., Skelly, M. B., Bouvier, J. et al., 2010, *MNRAS*, 402, 1426
- Drew, J. E., Gonzalez-Solares, E., Greimel, R., et al., 2014, *MNRAS*, 440, 2036
- Fang, M., van Boekel, R., Wang, W., et al., 2009, *A&A*, 504, 461
- Fedele, D., van den Ancker, M. E., Henning, Th., Jayawardhana, R., Oliveira, J. M., 2010, *A&A*, 510, 72
- Feigelson, E. D., Montmerle, T., 1999 *ARA&A*, 37, 363
- Fernandes, B., Gregorio-Hetem, J., Montmerle, T., Rojas, G., 2015, *MNRAS*, 448, 119
- Fernandes, B.; Montmerle, T., Gregorio-Hetem, J., Santos-Silva, T., 2019 *A&A*, 628, 44
- Fischer, W. J.; Padgett, D. L., Stapelfeldt, K. L., Sewilo, M., 2016, *ApJ*, 827, 96
- Gaia Collaboration, Brown, A. G. A., Vallenari, A., Prusti, T. et al. 2018a *A&A*, 616, 1
- Gaia Collaboration, Babusiaux, C., van Leeuwen, F., Barstow, M. A. et al. 2018b, *A&A*, 616, A10

- Galli, P. A. B., Bertout, C., Teixeira, R., Ducourant, C., 2013, *A&A*, 558, 77
- Gregorio-Hetem, J., Lépine, J. R. D., Quast, G. R., Torres, C. A. O., de La Reza, R., 1992, *AJ*, 103, 549
- Gregorio-Hetem, J.; Hetem, A. 2002, *MNRAS*, 336, 197
- Gregorio-Hetem, J. 2008, *Handbook of Star Forming Regions*, Vol. II, p. 1
- Gregorio-Hetem, J., Montmerle, T., Rodrigues, C. V. et al., 2009, *A&A*, 506, 711
- Gregorio-Hetem, J., Hetem, A., Santos-Silva, T., Fernandes, B., 2015, *MNRAS*, 448, 2504
- Gregorio-Hetem, J., Fernandes, B., Santos-Silva, T., Montmerle, T., 2016, in *“Interstellar Clouds to Star-forming Galaxies: Universal Processes?”*, *Proceedings IAU Symposium No. 315*, P. Jablonka, Ph. André & F. Van der Tak, eds.
- Haisch, K. E., Lada, E. A., & Lada, C. J., 2001, *ApJ*, 553, L153
- Hashimoto, J., Tsukagoshi, T., Brown, J. M. et al. 2015, *ApJ*, 799, 43
- Hashimoto, J., Dong, R., Kudo, T. et al. 2012, *ApJ* 758, 19
- Hernández, J., Hartmann, L., Calvet, N., et al. 2008, *ApJ*, 686, 1195
- Hetem, A. & Gregorio-Hetem, J., 2007, *MNRAS*, 382, 1707
- Hetem, A., Gregorio-Hetem, J., 2019, *MNRAS*, 490, 2521
- Kalari, V. M., Vink, J. S., Drew, J. E., et al., 2015, *MNRAS*, 453, 1026
- Keppler, M., Benisty, M., Müller, A., et al. 2018, *A&A*, 617, A44
- Koenig, X. P., Leisawitz, D. T. 2014, *ApJ*, 791, 131
- Maíz Apellániz, J., 2006, *AJ*, 131, 1184
- Marigo P. et al., 2017, *ApJ*, 835, 77
- Martínez-Arnáiz R.; López-Santiago, J.; Crespo-Chacón, I.; Montes, D., 2011 *MNRAS*, 414, 2629
- Mendes de Oliveira, C., Ribeiro, T., Schoenell, W., et al., 2019, *MNRAS*, 489, 241
- Molino A., Benítez, N., Moles, M. et al., 2014, *MNRAS*, 441, 2891
- Müller, A., Keppler, M., Henning, Th. et al. 2018, *A&A*, 617, L2
- Onishi, T., Nishimura, A., Ota, Y., et al. 2013, *PASJ*, 65, 78
- Preibisch, T., 2012, *Research in Astronomy and Astrophysics*, 12, 1
- Rebull, L. M., Padgett, D. L., McCabe, C.-E. et al., 2010, *ApJS*, 186, 259
- Riaud, P.; Mawet, D.; Absil, O.; Boccaletti, A.; Baudoz, P.; Herwats, E.; Surdej, J., 2006, *A&A*, 458, 317
- Santos-Silva, T., Perottoni, H.D., Almeida-Fernandes, F. et al. , 2020 *A&A*, (in preparation)
- Santos-Silva, T.; Gregorio-Hetem, J.; Montmerle, T.; Fernandes, B.; Stelzer, B., 2018 *A&A*, 609, 127
- Shevchenko, V. S., Ezhkova, O. V., Ibrahimov, M. A. et al. 1999, *MNRAS*, 310, 210
- Siess L., Dufour E., Forestini M., 2000, *A&A*, 358, 593
- Venuti, L., Bouvier, J., Flaccomio, E., Alencar, S. H. P., et al. 2014, *A&A*, 570, 82
- Wiramihardja et al., 1986, *PASJ* 38, 395
- Wright, E. L., Eisenhardt, P. R. M., Mainzer, A. K., et al. 2010, *AJ*, 140, 1868